Weaver, P.P.E., Schmincke, H.-U., Firth, J.V., and Duffield, W. (Eds.), 1998
Proceedings of the Ocean Drilling Program, Scientific Results, Vol. 157

14. EMPLACEMENT OF ASH LAYERS RELATED TO HIGH-GRADE IGNIMBRITE P1 IN THE SEA AROUND GRAN CANARIA[1]

Armin Freundt[2] and Hans-Ulrich Schmincke[2]

ABSTRACT

Drilling into the volcaniclastic apron around Gran Canaria at Sites 953 (68 km northeast of the island), 955 (56 km southeast), and 956 (60 km southwest) reached ash layers that stratigraphically correspond to the middle Miocene change from basaltic to felsic volcanism marked by the rhyolite-trachyte-basalt mixed ignimbrite cooling Unit P1 on the island. The P1 ignimbrite eruption produced a tephra volume of ~80 km^3 (DRE), including the submarine ashes. Compositionally very heterogeneous, 44- to 86-cm-thick ash beds, the "P1 layers," mark the first appearance of P1 pyroclastic material in the cores. Component particles common to all sections are abundant anorthoclase and oligoclase, minor amphibole, Fe-Ti oxide, apatite and zircon crystals, mostly vesicular aphyric basaltic tachylite, mostly dense trachyandesitic tachylite with oligoclase and augite microphenocrysts, and variably vesicular vitric particles of rhyolitic or trachytic composition shown by phenocrysts, which have been altered to clay. These P1-derived components are mixed with 10%–70% accidental clinopyroxene (identified by composition), holocrystalline angular epiclastic basalt fragments, mostly vesicular hyaloclastite-derived basaltic vitric fragments extremely abundant at Site 956, and a mixed population of shallow-water, benthic and planktonic fossils and bioclasts.

Vertical compositional and textural variations of the P1 layers reflect two depositional cycles at Sites 953 and 956 and three cycles at Site 955. Each cycle begins with fines-poor, very crystal-rich (up to 65%), massive coarse ash that contains shallow-water bioclasts and benthic fossils (<5%), and gradually changes upward toward fine ash rich in planktonic fossils (up to 36%), well stratified to cross-bedded with alternating crystal- and fossil-rich laminations. The upper cycles are thinner, overall finer grained (though tachylite lapilli-rich basal zones occur), and contain higher fractions of planktonic fossils and clayey matrix than the lower ones. These deposits were emplaced by turbidity currents of decreasing strength that were generated during the course of the P1 eruption, because the upward decrease in feldspar crystals coupled with an increase in the coeval basalt fraction through the P1 layers corresponds to the compositional zonation of the P1 ignimbrite on land. The large volume of foreign material in the P1 layers, derived from the shelf and upper flank of the island, suggests massive slumping off the shelf feeding the turbidity currents, possibly triggered by entrance of the hot ash flows into the sea. Ash flow-seawater interaction along the deeply incised northern coast differed from that in the low-relief south by producing peculiar microcrystalline fragments abounding at Site 953 but absent from the southern sites and without equivalent on land.

Volcaniclastic turbidite beds above the P1 layers also contain P1 material but are separated by pelagic fossil claystone beds representing periods of order 10^2 years. The first epiclastic detritus from the P1 welded ignimbrite occurs together with the first crystals relating to subsequent ignimbrite R.

INTRODUCTION

Volcanic activity on Gran Canaria, the central island of the Canarian Archipelago (Fig. 1) in the east central Atlantic, lasted from at least 15 Ma to the present. The major constructive phase, however, was the Miocene magmatic cycle from ~15 to 9 Ma, which included the formation of the basaltic shield (i.e., >90 vol% of the island) and the subsequent eruption of more than 800 km^3 of highly evolved magmas from the central Tejeda caldera, now exposed as the (partly peralkaline) rhyolitic to trachytic Mogán Group (14–13 Ma) and trachyphonolitic Fataga Group (13–9 Ma) rocks (Schmincke 1976, 1993; Hoernle and Schmincke, 1993).

At 14 Ma, basaltic submarine through subaerial volcanism was suddenly replaced by the eruption of the prominent rhyolite-trachyte-basalt, mixed welded ignimbrite P1, forming the base of the Mogán Group. P1 is overlain by the less voluminous rhyolite-basalt zoned ignimbrite R. Preceeding P1, only two local precursory eruptions of rhyolitic and trachytic magmas occurred near the end of the basaltic shield phase. Intermediate to evolved plutonic xenoliths in P1 document earlier production inside the island of differentiated magmas which did not, however, erupt on the subaerially exposed part of Gran Canaria.

Drilling into the volcaniclastic apron around Gran Canaria at Sites 953 (68 km northeast off the coast), 955 (56 km southeast), and 956 (60 km southwest) of Ocean Drilling Program (ODP) Leg 157 (Fig. 1) recovered tephra layers stratigraphically equivalent to the Miocene magmatic phase. Our study of core samples collected from the stratigraphic interval representing the 14-Ma change in magmatic evolution and eruptive style aims to (1) determine whether evolved magmas have been erupted, or evolved plutons been exposed, on the submarine flanks prior to eruption of P1; (2) find evidence for the type of interaction of the voluminous hot ash flows with seawater upon entrance into the ocean; and (3) identify the mode of emplacement of the submarine ash layers and the sources of the material accumulated in them. Here we report preliminary results of work in progress, mainly focussing on the third topic; a more comprehensive account will be given at a later stage.

Analytical Methods

Polished thin sections were prepared from all samples analyzed for this study, which are listed in Table 1. Petrographic studies involved modal analyses (point counting, 500 points per thin section) and measuring the grain-size distribution of feldspar crystals (300–400 grains per thin section), which are most suitable for comparison between samples, because they are present in all samples (also on land), they are not altered, and they are reliably measured in thin section because of their simple shape. Bulk grain-size distributions of four unsolidified samples from Hole 955A were determined by wet sieving (down to 90 µm) and by laser granulometry (down to 1 µm). Electron microprobe analysis of mineral phases, using an accelerating voltage of 15 kV, a beam current of 20 nA for pyroxene and 10 nA for amphibole with focused beam but a current of 10 nA with de-

[1]Weaver, P.P.E., Schmincke, H.-U., Firth, J.V., and Duffield, W. (Eds.), 1998. *Proc. ODP, Sci. Results*, 157: College Station, TX (Ocean Drilling Program).
[2]GEOMAR Forschungszentrum, Wischhofstr. 1-3, D-24148 Kiel, Federal Republic of Germany. afreundt@geomar.de

Prior Chapter Contents Next Chapter

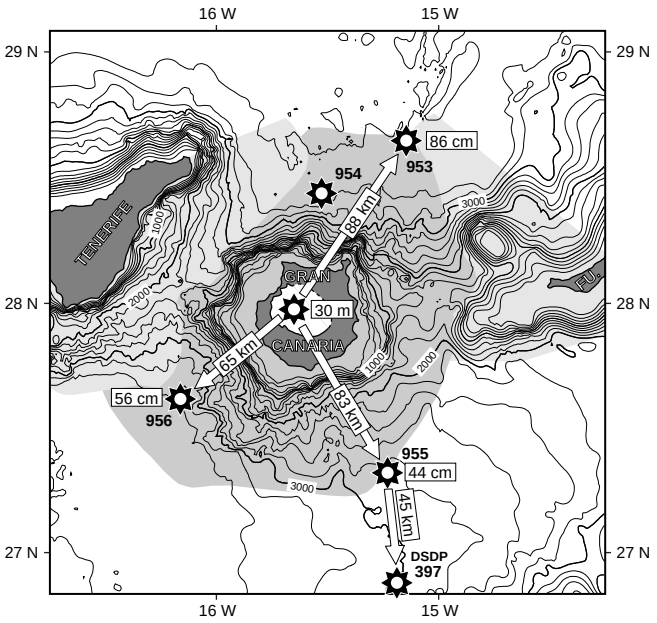

Figure 1. Map showing the position of ODP Sites 953, 954, 955, and 956, and DSDP Site 397 around Gran Canaria. Distance of each site to the approximate center of eruption in the Tejeda caldera (white) is given in the arrows; thicknesses of the P1 layer are shown at each site. The average ignimbrite thickness on land is ~30 m. The P1 stratigraphic interval is absent at Site 954. The seismically defined volcaniclastic apron of Gran Canaria (gray shading) is overlapped by the younger apron of Tenerife in the west, but overlies the older apron of Fuerteventura (FU.) in the east (both in light gray shading). Depth contours are shown in 200-m intervals. Based on bathymetric and seismic apron map of Funck (1995).

Table 1. List of samples analyzed for this study.

Core, section, interval (cm)	Depth (mbsf)	Ash layer
157-953C-		
70R-1, 29-33	841.13	A6
70R-1, 75-78	841.58	A4
70R-2, 64-68	842.67	A1
70R-2, 117-120.5	843.21	P1
70R-2, 120.5-124	843.25	P1
70R-2, 124-127	843.28	P1
70R-2, 127-130	843.31	P1
70R-3, 4-7	843.53	P1
70R-3, 9-11	843.57	P1
70R-3, 12-15.5	843.61	P1
70R-3, 15.5-19	843.65	P1
70R-03, 19-23	843.69	P1
157-955A-		
60X-3, 140-144.5	565.34	P1
60X-3, 145-146.5	565.36	P1
60X-3, 147.5-149	565.39	P1
60X-4, 22	565.62	P1
60X-4, 23.5	565.63	P1
60X-4, 25	565.65	P1
60X-4, 26	565.66	P1
60X-04, 27-29	565.69	P1
157-956B-		
43R-2, 2-5	562.65	A5
43R-2, 50-53	563.13	A3
43R-2, 81-84	563.44	A2
43R-2, 115-117	563.77	P1
43R-2, 118-121	563.81	P1
43R-2, 142-145	564.05	P1
43R-3, 0-5	564.10	P1
43R-3, 5-9	564.15	P1
43R-3, 118-120	565.30	B2
43R-4, 61-65	566.25	B2

focused beam for feldspars, was used to support stratigraphic correlations of core samples with deposits on land.

IGNIMBRITE P1 ON LAND

We have studied the middle Miocene (13.9 Ma) composite ignimbrite cooling unit P1 in great detail on land to reveal its petrogenetic, eruption, and emplacement history (Freundt and Schmincke, 1992, 1995a, 1995b). We briefly summarize characteristics of P1 relevant to the understanding of the submarine ash layers investigated here.

P1 is zoned from a lower rhyolite-trachyte mixed tuff with a very high content of feldspar crystals through a central rhyolite-basalt mixed tuff to slightly rhyolite-contaminated basaltic tuff at the top (Fig. 2). The basaltic tuff is slightly quenched against the felsic tuff; the holocrystalline, intensely flow-aligned texture of its dominant densely welded zone changes to microcrystalline and tachylitic texture at its moderately to poorly welded top. Cooling structures are continuous across compositional and depositional boundaries, suggesting emplacement of the entire cooling unit in rapid succession. The entire P1 tuff, including the basaltic tuff, was emplaced all across the island by very hot ash flows that erupted from ring-fissures inside the Tejeda caldera and extended beyond the coastline; no evidence for associated plinian or co-ignimbrite fallout is preserved on land. P1 is composed of four component magmas mixed in vertically varying proportions.

1. P1 rhyolite phenocrysts comprise millimeter-sized zoned anorthoclase crystals (75%–92% of the phenocryst fraction), edenitic amphibole, Fe-Ti oxides, apatite, and zircon; rare biotite is included in edenite.
2. P1 trachyte to sodic trachyandesite (58–66 wt% SiO_2) contains oligoclase phenocrysts with typical coarsely resorbed zones, associated with augite, orthopyroxene, Fe-Ti oxides, and apatite as well as late-formed richteritic amphibole. A rare type of sodic trachyandesite contains more calcic plagioclase and kaersutitic amphibole.
3. Volumetrically subordinate P1 Na-poor trachyandesite (55.5–59 wt% SiO_2) contains plagioclase, augite, orthopyroxene, Fe-Ti oxide, and apatite crystals.
4. P1 basalt (47.2–49.5 wt% SiO_2) is nearly aphyric with <2% phenocrysts of calcic plagioclase, diopside, Fe-Ti oxides, olivine (all iddingsitized), and accessory apatite, and typically contains rhyolite-derived anorthoclase crystals with marginal to overall fingerprint resorption.

In addition, P1 contains mainly gabbroic cogenetic cumulate fragments, lithic fragments of shield basalt, and coarsely crystallized plutonic fragments of gabbroic to syenitic but mostly intermediate composition in vertically varying abundance (Fig. 2).

Cooling Unit R, which overlies P1 (Fig. 2), is also zoned from basal rhyolite that contains phenocrysts of oligoclase, amphibole, augite, rare hypersthene, oxides, apatite and zircon, to basaltic trachyandesite at the top. Two local occurrences of evolved volcanic rocks that underlie P1 in the west of the island (Fig. 2) are (1) a rhyolite to basaltic andesite zoned ignimbrite containing sodic plagioclase, augite, minor amphibole, Fe-Ti oxides, apatite, and zircon, and (2) a basaltic scoria and ash flow deposit with comagmatic trachytic inclusions containing sodic plagioclase, augite, orthopyroxene, Fe-Ti oxides, and traces of apatite and zircon.

MARINE ASH LAYERS RELATED TO IGNIMBRITE P1

Major 44- to 86-cm-thick packages of ash layers stratigraphically equivalent to ignimbrite P1, below called “the P1 layers,” mark the base of tephra Unit IV, defined by Schmincke, Weaver, Firth, et al.

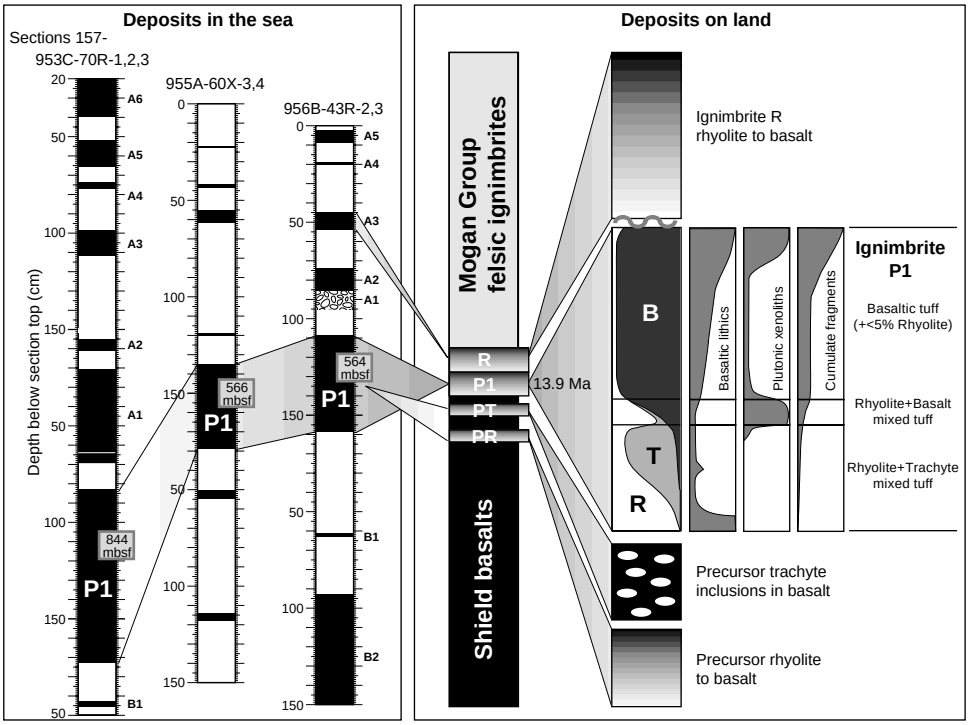

Figure 2. Correlation between ash deposits in the sea and on land. **Left:** Schematical profiles of core sections drilled at Holes 953C, 955A, and 956B, stratigraphically correlated to deposits on land using mineral compositions. Ash layers are in black, claystone in white. The depth below seafloor of the P1 layers is indicated. Layer A1 in Hole 956B is a conspicuous breccia of large claystone fragments in a volcanic ash matrix. Average Miocene sedimentation rates from Schmincke, Weaver, Firth, et al. (1995) imply time breaks between ash layers of 200–400 yr per centimeter intercalated claystone. **Right:** Schematical column of shield basalts capped by the Mogán Group felsic ignimbrite sequence, which together with the overlying Fataga Group volcanics represent the Miocene magmatic cycle of Gran Canaria (Schmincke, 1982, 1993). Compositionally zoned or mixed cooling units that mark the change from basaltic to felsic volcanism are emphasized and illustrated in the column to the right. For the P1 ignimbrite, vertical variations in the proportions of the major magmatic components rhyolite (R), trachyte to sodic trachyandesite (T), and basalt (B) are shown as well as the abundance of accidental components (visual field estimates). The age of P1 is 13.9 Ma after Bogaard and Schmincke (Chap. 11, this volume). Reworking and local erosion at the top of P1 indicate a break in volcanic deposition that preceded emplacement of ignimbrite R.

(1995), in Holes 953C, 955A, and 956B (Fig. 2). Additional ash beds containing P1 material are separated by nannofossil claystone higher in the respective sections, indicating major time breaks of order 10^2 years in the submarine deposition of volcanic material.

Stratigraphic Correlations

We use chemical compositions of minerals to correlate the marine ash beds with the volcanic deposits on land. The compositions of the major mineral phases feldspar, amphibole, and clinopyroxene are distinct for the volcanic rocks at the boundary between shield basalts and Mogán Group felsic rocks.

Feldspar compositions from the P1 layers in all three holes plot into the feldspar compositional fields of P1 rhyolite and trachyte (Fig. 3A, B). Crystals of intermediate composition could be derived from trachyandesitic rocks of P1 or from cumulates, and rare calcic feldspars from basaltic rocks. Rhyolite-derived feldspars dominate in samples from Holes 955A and 956B, whereas approximately equal abundances of rhyolite- and trachyte-derived feldspars are found in samples from Hole 953C (Fig. 3A). Feldspars in ash layers above the P1 layer of Hole 956B are partly of P1 rhyolite composition, some are intermediate to calcic, but most (especially in Sample 157-956B-43R-2, 50–53 cm) have a composition identical to ignimbrite R feldspars (Fig. 3C). Feldspars from ash layers below the P1 layer in Hole 956B are intermediate to calcic, but some crystals from Sample 157-956B-43R-3, 118–120 cm, plot into the feldspar compositional fields of the evolved precursor rocks.

Amphibole crystals in the P1 ash layers of the three holes overlap in composition with amphibole phenocrysts of the P1 rhyolite (Fig. 4A–D). Ash beds above P1 in Hole 956B contain amphiboles derived from P1 rhyolite, but also from ignimbrite R (Sample 157-956B-43R-2, 50–53 cm). Amphiboles in ash layers below P1, but also some high-Al amphibole crystals from an ash layer above P1 (Sample 157-956B-43R-2, 81–84 cm), are not related to ignimbrite P1 or its associated deposits (Fig. 4E, F). Schmincke and Segschneider (Chap. 12, this volume) have interpreted the occurrence of sandstone beds extremely rich in amphibole of this composition as tsunami deposits derived from La Gomera. Amphiboles of this composition occur sporadically throughout tephra units corresponding to the lower Mogán Group at Site 956 (Sumita and Schmincke, Chap. 15, this volume).

Only rare clinopyroxene crystals in the P1 layers have the composition of pyroxene phenocrysts from P1 trachyte or evolved precursor rocks, or are intergrown with intermediate plagioclase and thus represent cumulate fragments. Almost all clinopyroxenes analyzed in the P1 ash samples have compositions appropriate for phenocrysts of basaltic rocks (Fig. 5) and must be xenocrysts derived from older shield basalts because (1) the almost aphyric P1 basalt could not have contributed so many pyroxene crystals, (2) in general, the pyroxenes have a higher Al_2O_3-content than the P1 basalt phenocrysts, and (3) some pyroxenes are phenocrysts in hyaloclastite-derived vesicular basaltic vitric fragments at Site 956. A xenocrystic origin is also supported by the high clinopyroxene fractions ($0.2 < X_{cpx} \leq 1$) in the ash layers, expressed as X_{cpx}= cpx/(cpx+am) obtained from modal analyses, which are only <0.1 in P1 felsic tuff on land (where cpx is trachyte-derived augite). Especially high values of $X_{cpx} > 0.65$ in P1 ash at Hole 956B coincide with a high content of highly vesicular basaltic vitric fragments; destruction of such particles during transport probably set free their pyroxene phenocrysts to accumulate in the P1 ash.

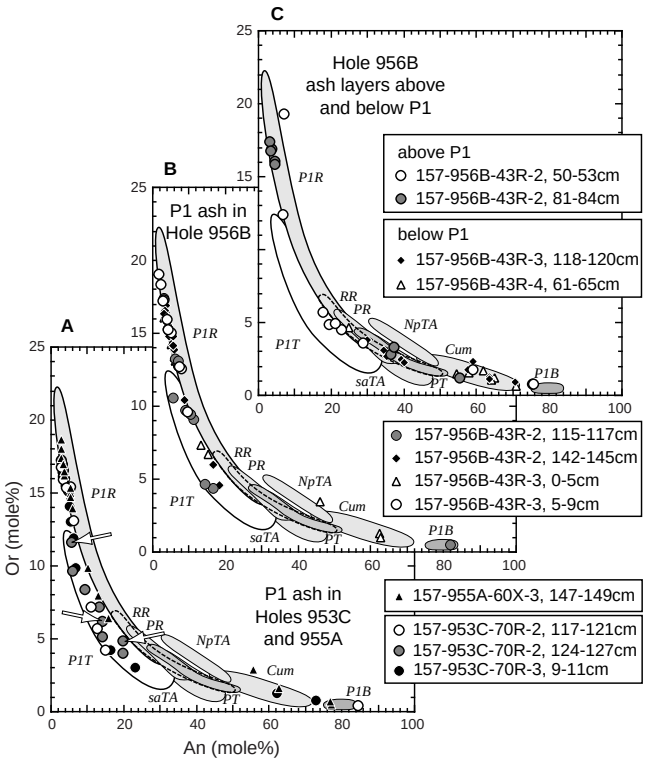

Figure 3. Feldspar crystal compositions from submarine ash samples compared to compositional fields for feldspars in the P1 and associated rocks on land: P1R = rhyolite of P1, P1T = trachyte through sodic trachyandesite of P1, P1B = basalt of P1, saTA = sodic amphibole-bearing trachyandesite of P1, NpTA = Na-poor trachyandesite of P1, Cum = cumulate fragments in ignimbrite P1, PR = precursor rhyolite, PT = precursor trachyte, and RR = rhyolite of ignimbrite R. Arrows in A point to feldspar phenocrysts in pale microcrystalline particles (MRT), which are apparently of trachytic composition.

Igneous Rock Fragments and Bioclasts in the P1 Ash Layers

Igneous particles of varying composition occur together with crystals in the ash layers, as discussed below.

Tachylitic Basaltic Particles

Tachylitic basaltic particles (TaB) are commonly vesicular (Pl. 1, Figs. 1, 2), some with round but most with irregularly shaped vesicles, and free of crystals except for occasionally included anorthoclase or oligoclase crystals derived from P1 rhyolite or trachyte. Larger tachylite particles in the P1 layers show textures typical of P1 basalt tuff (Pl. 1, Fig. 2), as discussed below. The abundance of round slightly vesicular tachylite in the P1 ashes suggests that they most likely represent P1 basalt, which constitutes about half of the ignimbrite on land. Angular dense tachylite particles containing minor plagioclase microlites also occur in the P1 layers and form a major component of submarine ashes underlying the P1 layers; we interpret these as fragments derived from older lavas.

Microcrystalline Basaltic Particles

Microcrystalline basaltic particles (MiB) are dense to coarsely vesicular and angular to irregular in shape. Anorthoclase crystals contained in some of these particles and a gradual transition between microcrystalline to tachylitic fragments suggest P1 basalt as their source.

Holocrystalline Basaltic Particles

Holocrystalline basaltic particles (HoB) are dense and always angular with slightly rounded edges. A wide range of textural and compositional types exists, differing in the degree of parallel alignment of plagioclase laths and in the ratio of opaque oxides to clinopyroxene, although the oxides commonly dominate. Such rocks occur as lithic

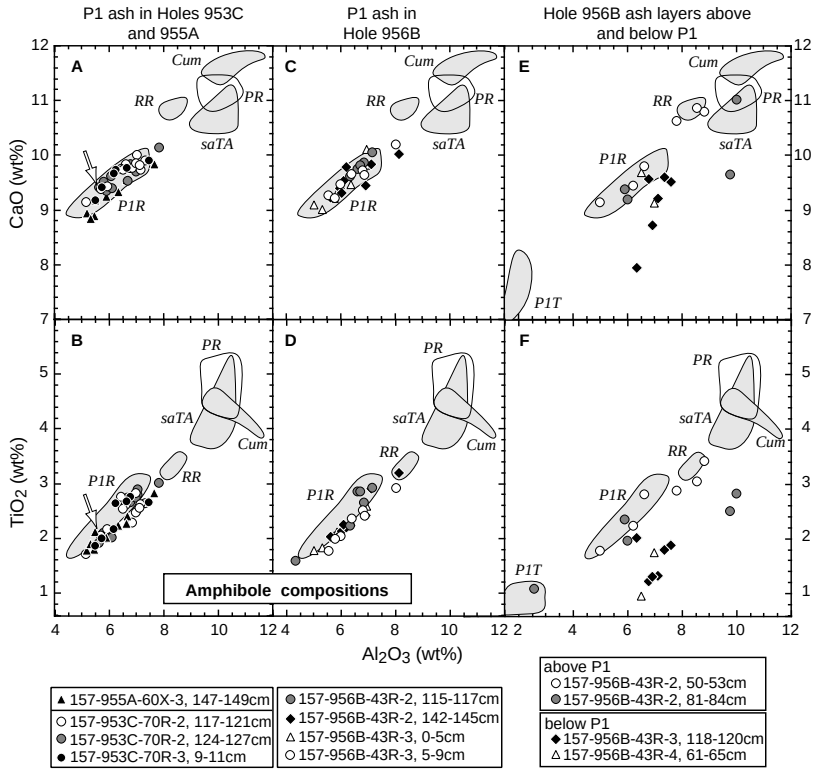

Figure 4. Amphibole crystal compositions from submarine ash samples compared with compositional fields for amphiboles in the P1 and associated rocks on land. Abbreviations as in Figure 3. Arrows = amphibole phenocryst in pale microcrystalline particle (MRT), which apparently has a rhyolitic composition.

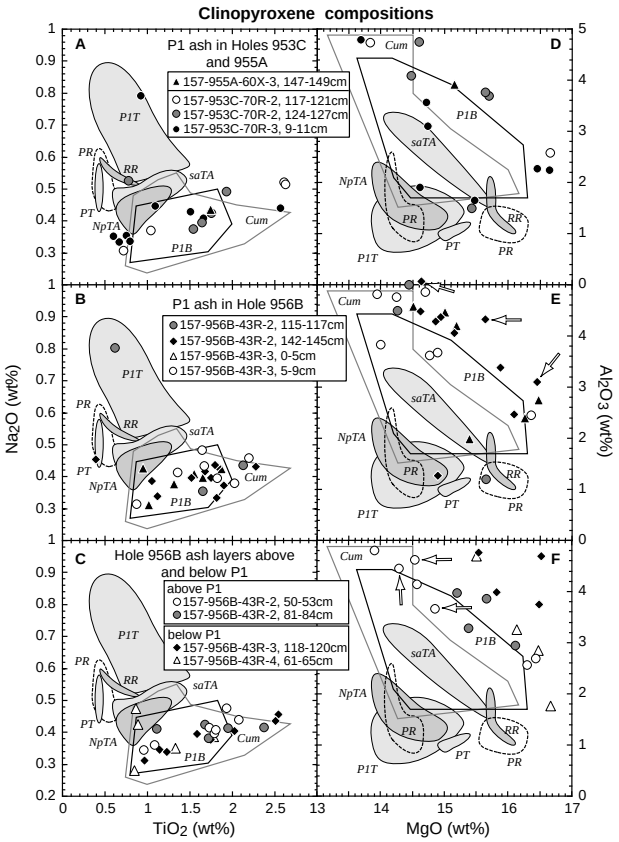

Figure 5. Clinopyroxene crystal compositions from submarine ash samples compared to compositional fields for pyroxenes in the P1 and associated rocks on land. Abbreviations as in Figure 3. Arrows = phenocrysts in vesicular basaltic vitric fragments (ViB).

fragments in the P1 basaltic tuff but differ from the P1 basalt itself, which is also holocrystalline in the center of the deposit on land but shows more intense flow-alignment of the plagioclase laths, clinopyroxene exceeding oxide microlites in abundance, and conspicuous red iddingsitized olivine microlites. Many of the HoB fragments have thin brownish alteration rims, which are possibly the result of subaerial oxidation. They therefore are interpreted as lithic material derived from land (Schmincke and von Rad, 1979; Schmincke and Segschneider, Chap. 12, this volume) and not coeval to P1 basalt.

Basaltic Vitric Fragments

Basaltic vitric fragments (ViB) are angular and dense to highly vesicular, with a well-sorted size range of round vesicles. Their mafic bulk composition is evidenced by the composition of pyroxene and plagioclase phenocrysts. The fragments appear mostly clear because the glass has been completely dissolved in situ, leaving only crystals and vesicle walls, which are probably preserved because they had already been palagonitized at an earlier stage. These particles abound below P1 and thus represent hyaloclastites of the submarine to emergent shield stage described by Schmincke and Segschneider (Chap. 12, this volume).

Trachyandesitic Tachylite

Trachyandesitic tachylite (TaT) of P1 differs from basaltic tachylite in that it is slightly brownish black, dense to coarsely vesicular with round vesicles, and contains relatively large stubby plagioclase, augite, and oxide crystals (Pl. 1, Fig. 1).

Vitric P1 Rhyolite or Trachyte Particles

Vitric P1 rhyolite or trachyte particles (VRT) are pale brown through olive-brown to dark brown and consist of clay minerals (rarely of zeolites) that have replaced all felsic glass. Their original character is suggested by phenocrysts of anorthoclase, amphibole and zircon (indicating P1 rhyolite) or of commonly resorbed oligoclase and augite (indicating P1 trachyte). A pumiceous texture of poorly sorted vesicle sizes is often preserved (Pl. 2, Figs. 2, 3), whereas other particles contain a network of dark lines suggesting a texture of collapsed vesicles (Pl. 2, Fig. 1), and still others are intensely lineated as in strongly stretched and compacted pumice (Pl. 2, Fig. 4).

Microcrystalline Rhyolitic or Trachytic Particles

Microcrystalline rhyolitic or trachytic particles (MRT) may contain the same mineral assemblages noted above. These particles are mostly gray with thin brown rims, angular, and often internally fractured (Pl. 1, Figs. 2, 3). Vesicles are rare. There is no flow banding in these particles, although flow banding in microcrystalline felsic P1 ignimbrite facies on land is intense down to microscopic scale.

Bioclasts

Bioclasts comprise planktonic globigerinoid (and rarely rotaliide) foraminifers and rare fish scales. Planktonic fossils are present in variable abundance throughout the ash layers. Benthic fossils such as *Amphistegina, Operculina,* sand-shelled, and other asymmetric foraminifers are enriched in certain layers and associated with bioclasts derived from shallow water such as thick Cc-bivalves, coralline algae, bryozoa, echinoid, sponge, snail, and *Serpulina* fragments.

HOLE 953C STRATIGRAPHY

The P1 layer at Site 953 occurs at 844 meters below seafloor (mbsf) at the base of Subunit IVC of Schmincke, Weaver, Firth, et al. (1995). We have subdivided the 86-cm-thick P1 layer into six units (A to F) on the basis of bedding characteristics and composition (Fig. 6).

Unit A

Coarse-grained massive ash layer A (4 cm thick) has a sharp, unconformable, erosive contact to the underlying fossil claystone, which contains admixed fragments and crystals from A, whereas a thin basal zone of A contains clayey matrix. Above this zone, layer A is well-sorted coarse ash lacking fine matrix; voids between particles are mostly filled by fine-grained to blocky calcite. Large feldspar crystals (Md = 280 µm; Fig. 7), and minor amphibole, clinopyroxene, Fe-Ti oxides, as well as traces of zircon and apatite constitute 65% of the coarse particles (Fig. 6), followed in abundance by holocrystalline basaltic fragments. Coarsely vesicular basaltic vitric shards are rare. Basaltic tachylitic through crypto- to microcrystalline particles that form a minor fraction probably represent P1 basalt. A large fraction of black to brownish tachylitic particles have P1 mafic trachyte to trachyandesite composition, as shown by abundant feldspar laths, augite, and Fe-Ti oxide crystals. Pale-brown zeolitized vitric particles are very rare. Conspicuous gray, angular rhyolitic and trachytic microcrystalline particles (Pl. 1, Fig. 3) occur as a minor component; their original composition is shown by included crystals (Figs. 3A, 4A, B). Fossils in A represent a mixture of mainly shallow-water, benthic, and fewer planktonic organisms.

Unit B

This is a 47-cm-thick massive ash layer with only vague bedding becoming more pronounced toward the top, where bedding is first de-

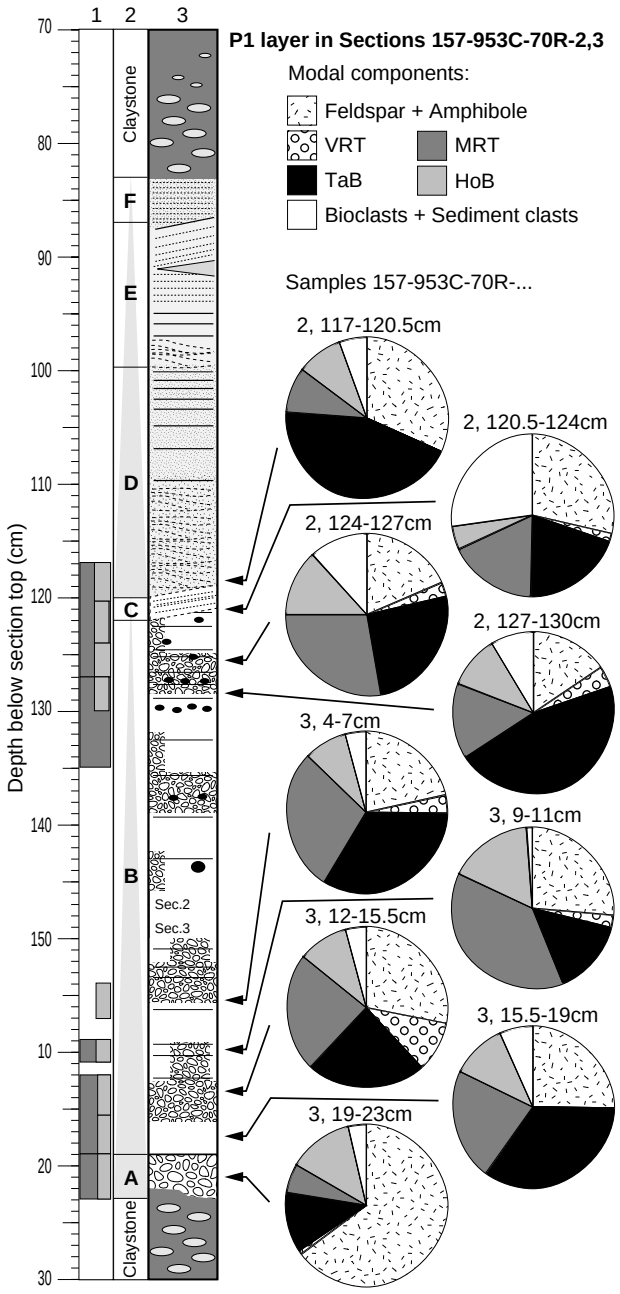

Figure 6. **Left:** Stratigraphic profile of the P1 layer in Hole 953C. Dark gray boxes = position of core samples, and light gray boxes = position of thin sections (Table 1). Subunits A to F, and the two depositional cycles (gray triangles) are marked in column 2. Column 3 is a graphic lithologic profile illustrating overall upward decreasing grain size and increasing lamination and cross-bedding. Black dots indicate occurrences of round tachylite particles several millimeters in diameter. **Right:** Pie charts of modal composition (calculated matrix free) of ash samples. Feldspar and amphibole crystals reflect the P1 rhyolite component. VRT = formerly pumiceous glassy, now variably devitrified and altered, rhyolitic-trachytic particles. TaB = tachylitic to cryptocrystalline basalt particles which are mainly P1 basalt, though some lithic tachylite may be present; trachyandesitic tachylite is not included here. MRT = microcrystalline particles of evolved composition. HoB = holocrystalline basaltic particles of xenolithic origin. Note the abundance of microcrystalline rhyolite-trachyte particles (MRT) in this section.

fined by zones of alternating grain size and finally by alternating crystal-rich and fossil-rich beds. The feldspar crystal size distributions (Fig. 7) reflect an overall decrease in grain size toward the top of layer B but several horizons enriched in millimeter-sized basaltic tachylitic (Pl. 1, Fig. 2) and felsic microcrystalline lapilli, which are abundant throughout layer B (Fig. 6), occur across the topmost 10

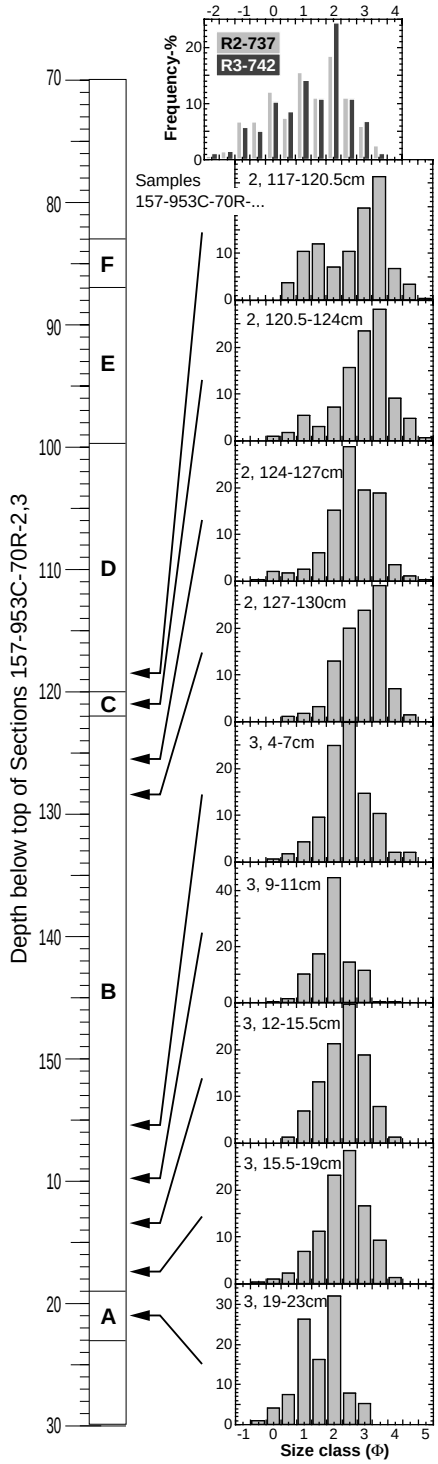

Figure 7. Histograms of feldspar crystal-size distributions of P1 ash samples in Hole 953C. The feldspar crystal-size distribution of felsic P1 tuff on land (Samples R2-737, R3-742) is shown for comparison at the top.

cm. Some of the basaltic tachylite particles have highly crenulated shapes closely resembling quenched basalt inclusions in P1 rhyolite-basalt mixed tuff on land. The crystal content is lower than in A and decreases upward from 30% to 16%. Holocrystalline basalt accounts for 8%–13% throughout the layer, and basaltic vitric shards are rare. Yellow-brown rhyolitic-trachytic vitric particles (Pl. 2) occur throughout layer B but are most abundant (up to 10%) in its lower part. There is no fine-grained matrix, but all particles are coated by clay minerals. Shallow-water, benthic, and planktonic organisms are mixed throughout layer B, but the planktonic globigerinoid foraminifers dominate in abundance toward the top.

Unit C

Thin Unit C is a conspicuous white band, its color being caused by abundant globigerinoid foraminifers and calcite matrix that probably replaces former fine-grained clastic matrix. It is a continuation of the alternating crystal- and fossil-rich layers at the top of Unit B but the fossil-rich layers now strongly dominate over the discontinuous, lensoid ash-rich layers. Ash particles are finer grained than at the top of B (Fig. 7), but comprise the same components. The contact with overlying coarser-grained ash layer D is sharp but wavy.

Unit D

Unit D is 20 cm thick and is dominated by tachylitic particles and feldspar crystals, which have a bimodal size distribution with a distinct coarse fraction (Fig. 7). Particles of microcrystalline rhyolite-trachyte, holocrystalline basalt, and fossils constitute minor components, and felsic vitric particles are very rare. Fossils again comprise a mixture of shallow-water, benthic but dominantly planktonic species. There is no fine-grained matrix, and interparticle voids are partially filled by zeolite rosettes. Low-angle cross-bedding and thin lamination of layer D become more pronounced with finer grain size toward the top.

Unit E

Unit E is a 13-cm-thick continuation of D, but is composed of still finer-grained, silty ash and shows laminations distinct by color changes. Parallel lamination to very low-angle bedding prevail in the lower part, but steeper cross-bedding and discontinuous layers occur in the upper half.

Unit F

The coarser grained base of Unit F rests in sharp wavy contact on top of E. Planar to weakly cross-bedded ash of F gradually mixes upward with fossil clay, which rapidly dominates until at >4 cm above base F, where ash components are no longer macroscopically recognized in the clay matrix. This level is defined as the top of the P1 layer, which is separated by 14 cm of fossil clay from the next ash layer A1.

Ash Layers Above P1

Layer A1 above P1 (Fig. 2) is a coarse ash containing abundant tachylite and crystals, minor holocrystalline basalt, and some microcrystalline and vitric felsic particles. Anorthoclase (also present in some tachylite fragments), amphibole, augite, oxides, zircon and apatite demonstrate that most of the volcanic material is derived from P1. Bioclasts make up 7% of the fragments and are dominated by mollusc shells that must have been derived from very shallow water.

Layer A4 consists of alternating, partly discontinuous, ash-dominated and fossil-dominated beds. Volcanic particles are mostly tachylite, crystals as in A1, holocrystalline basalt, and rare brownish vitric fragments. The fossil assemblage is entirely planktonic/nektonic. Thicker ash beds of A4 are matrix free, but thinner beds contain clay. Larger scale mixing of A4 ash with overlying fossil clay occurs at the top of the layer.

Layer A6 shows similar large-scale mixing at its base. A6 is very similar to A4 in terms of grain size, bedding, and volcanic and fossil components. It differs in containing shallow-water derived bioclasts as well as brown phlogopite crystals and two types of amphibole: a majority of brownish crystals petrographically identical to edenite in P1 rhyolite and a minority of green crystals, which could be derived from ignimbrite R.

HOLE 955A STRATIGRAPHY

The P1 layer has been recovered from 567 mbsf in this hole, where it marks the base of Unit IV of Schmincke, Weaver, Firth, et al. (1995). We have distinguished eight Subunits A–H in the 44-cm-thick P1 layer in Hole 955A (Fig. 8). Stratigraphically equivalent core sections from Holes 953C and 956B are all solidified cemented rocks, but the material in 955A is commonly unsolidified, except for some centimeter-thick indurated zones parallel to the bedding, but apparently not related to bed boundaries.

Unit A

Coarse-ash Unit A is 24 cm thick and massive with few millimeter-thick intercalated silt beds. It overlies fossil claystone in sharp contact, but admixed clay forms the fine-grained matrix across the lower few millimeters. The matrix also contains dissolved or zeolitized cuspate basaltic shards, but upsection, most of the fine-grained matrix is replaced by zeolites. The bulk ash grain size distributions (Fig. 9) show pronounced maxima at ~250 µm (+2 ϕ), but a flat distribution across the grains <60 µm (+4 ϕ), which account for 16–36 wt%. The basal 1 cm of Unit A is vastly dominated by angular holocrystalline basaltic fragments accompanied by calcic plagioclase and clinopyroxene crystals. Sodic plagioclase is rare in this zone, but increases upward in abundance; at >1 cm above base it is accompanied by amphibole, augite, oxides, zircon and apatite, and rare phlogopite. The feldspar crystals in Unit A are very fine grained (Fig. 9) with a median size of 90 µm, in contrast to the abundant and large crystals at the base of the P1 layer in the other two holes. Many of the abundant tachylite fragments are marginally altered and thus represent older basalts. Others contain larger plagioclase and augite crystals typical of P1 trachyandesite so that only a minor fraction of the tachylites can be attributed to the P1 basalt. About 10% of the particles are angular, dense, largely crystallized basaltic vitric fragments rich in small plagioclase microlaths, mostly with flow lineation, together with opaque oxides and rare clinopyroxene. Rare crystalline fragments of mosaic-textured sodic plagioclase with clinopyroxene and opaque oxide, some also with amphibole, probably have a syenitic composition. Fossils near the base of Unit A are globigerinoid foraminifers, mostly incorporated from underlying fossil clay, and are associated with benthic and shallow-water bioclasts.

Unit B

Unit B is a 2.5-cm-thick layer that contains abundant millimeter-sized vesicular round basaltic tachylite lapilli in silty matrix. It is overlain in sharp contact by Unit C.

Unit C

Unit C is a 3-cm-thick, fine-grained massive ash, which has a clayey matrix containing abundant globigerinoid foraminifers. The ash particles are abundant vesicular basaltic vitric fragments and

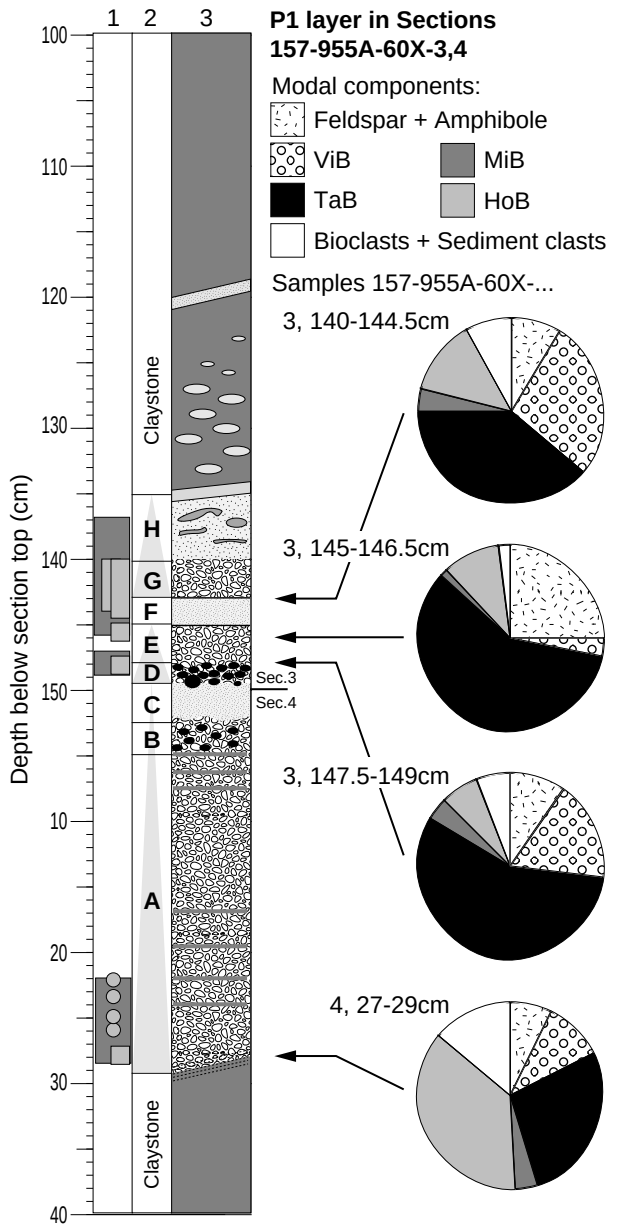

Figure 8. **Left:** Stratigraphic profile of the P1 layer in Hole 955A, divided into Subunits A to H. Other features as in Figure 6. Gray lines in Subunit A = fine partings, and gray lumps in Subunit H = clay clasts. **Right:** Modal composition of ash samples. ViB = basaltic vitric fragments, and MiB = basaltic microcrystalline particles. Other components as in Figure 6. Note the abundance of epiclastic basalt fragments (HoB) at the base, whereas tachylite (TaB) dominates higher in the section.

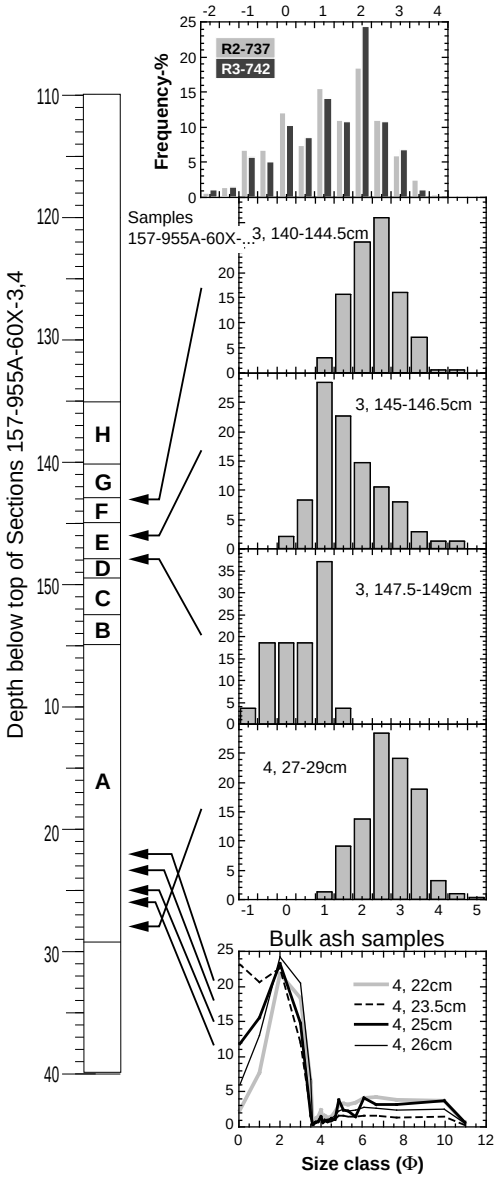

Figure 9. Histograms of feldspar crystal-size distributions of P1 ash layer in Hole 955A. The feldspar crystal-size distribution of felsic P1 tuff on land is again shown for comparison at the top. Bulk ash grain-size distributions of four samples from lower Unit A (lowermost histogram) show distinct maxima at +2 ϕ (similar to the feldspar distributions) and a flat distribution across the finer size range.

shards and rare holocrystalline basaltic fragments. Some large tachylite lapilli, which abound in overlying Unit D, occur in the topmost zone of layer C, into which they were probably mixed during emplacement of Unit D. The contact between Units C and D is sharp but very irregular.

Unit D

Unit D is only 1 cm thick, but contains abundant, mostly subspherical tachylite lapilli, normally graded from 5 mm diameter at the base to ~1 mm at the top. Mantled and composite tachylite particles (Pl. 1, Fig. 2), large sintered ash aggregates, tachylite with included anorthoclase, and oligoclase or highly inflated rhyolite are identical to those in moderately to poorly welded P1 basalt tuff on land. The coarse ash to lapilli size fraction also includes large crystals of anorthoclase and resorbed oligoclase, with a median size larger than in P1 tuff on land (Fig. 9), as well as holocrystalline basalt fragments. The typical P1 crystal assemblage is present with anorthoclase (intergrown with edenite), oligoclase (intergrown with augite), amphibole (with included biotite), augite, and oxide intergrown with zircon. The fine-grained matrix contains abundant vesicular basaltic shards; much of the matrix has been replaced by calcite. Fossils include planktonic, benthic and shallow-water species.

Unit E

Unit E is 3 cm thick and is dominated by basaltic tachylite particles of the same types as in Unit D, though smaller (<0.7 mm). A trachyandesitic composition of some tachylite fragments is indicated by feldspar and augite crystals. Sodic feldspar crystals account for 20% of the sand-size fraction; their size distribution shows a distinct fine tail but a cut-off at the coarse side, which would be complemented by the distribution found in Unit D (Fig. 9). The feldspars are accompanied by the other minerals typical of P1 rhyolite and trachyte. Holocrystalline basalt and vesicular basaltic vitric fragments form a minor fraction (12%) of the particles. Brown-olive rhyolitic and trachytic vitric material occurs as particles up to 2 mm in size, with variable pumice textures, and as rare glass rims around crystals. The fine-grained matrix of Unit E is mainly composed of shard-like fragments altered to clay and identical in appearance to the brownish vitric particles, but it also contains abundant clear vesicular or cuspate basaltic shards. We therefore interpret the matrix to represent a mixture of vitric felsic and basaltic ash. The fossil content of layer E is restricted to a few percent of small planktonic foraminifers dispersed in the matrix.

Unit F

Massive Unit F is only 2 cm thick and sharply bounded by planar to slightly wavy contacts at bottom and top. It consists of ~50% cuspate vesicular basaltic shards (<100 µm) dispersed in a matrix of clay, which shows textures of formerly fine ash particles. Small plagioclase crystals and fragments, and rare opaque oxides and pyroxenes occur in trace amounts (<2%) as do the few small globigerinoid foraminifers, mainly concentrated near the top of the bed. About one-third of the shards consists of brown sideromelane, only locally altered to zeolite, whereas the glass has dissolved from the majority of the shards, only locally being replaced by calcite. Optical extinction angles indicate a plagioclase composition of ~An_{60}, supporting the conclusion that the shards represent mafic vitric fragments.

Unit G

Overlying 3-cm-thick massive Unit G is a well-sorted, matrix-free medium ash dominated by tachylite and moderately vesicular to dense, partially crystallized basaltic vitric fragments in about equal abundance. Rare basaltic vitric particles, and patches within particles, have preserved sideromelane, but the glass is primarily dissolved. The texture of the tachylitic particles, and occasionally included anorthoclase, indicate that they represent P1 basalt. Holocrystalline basaltic lithics make up 10% of the particles. Another 10% fraction is formed by the crystals: anorthoclase and oligoclase, amphibole (with included biotite), augite, oxides, zircon, and apatite. The median size of feldspar crystals is 120 µm with a narrow distribution (Fig. 9). A minor component is olive-brown vitric particles with pumiceous or collapsed texture, also occurring as rims around amphibole and other crystals. Almost all inter- and intraparticle pores are filled by recrystallized calcite. All particles are coated by thin rims of clay. The rare fossils comprise a mixed planktonic, benthic, and shallow-water assemblage.

Unit H

Unit G grades into 5-cm-thick ash layer H, which is compositionally identical to G, but is finer grained and contains a matrix of ~10 µm angular brown particles mostly composed of clay minerals, which probably represent former vitric ash. Ash bed H is intensely mixed with fossil clay in its upper half and capped by a 5-mm-thin continuous yellow clay band marking the top of the P1 layer in Hole 955A.

The conspicuous microcrystalline rhyolitic and trachytic particles (MRT) observed in the P1 ash of Hole 953C do not occur in Hole 955A. Those rare microcrystalline particles that are present (Fig. 8) are of basaltic composition.

HOLE 956B STRATIGRAPHY

The P1 layer in Hole 956B, 564 mbsf at the base of Unit IV (Schmincke, Weaver, Firth, et al., 1995), is 56 cm thick and divided into sublayers A–F (Fig. 10).

Unit A

Unit A is a 2- to 3-cm-thick unit that rests with a concave-up curved but sharp boundary on the underlying fossil claystone. The coarse-grained (~800 µm), massive, well-sorted ash is dominated by almost 50% crystals (similar to the basal unit in Hole 953C) of sodic feldspar, amphibole (with included biotite), augite, oxide, apatite, and especially abundant and large zircon. Highly vesicular basaltic vitric fragments account for 20% of the particles, and holocrystalline basaltic fragments occur almost in the same abundance. Tachylitic and microcrystalline basaltic particles form a minor fraction, and rare trachyandesitic tachylite also occurs. Pale-brown vitric particles (Pl. 2) showing vesicle textures, intense internal lineations, or collapsed-pumice textures are variably devitrified: some are crystallized to platy feldspar or clusters of opaque oxide minerals, some are completely zeolitized, and others are replaced by calcite. Their phenocryst assemblages indicate both P1 rhyolite and trachyte compositions. There is no fine-grained clastic matrix, but zeolite rosettes partly fill interparticle voids. The mixed fossil assemblage comprises benthic, planktonic, and shallow-water bioclasts. Many of the large fossils as well as large crystals and basaltic vitric particles are dissected by jigsaw fractures that probably formed by in situ fragmentation during compaction.

Unit B

A gradual transition from light-colored Unit A into dark greenish black Unit B reflects the increasing abundance of tachylite particles and decrease of the crystal (mainly feldspar) fraction to 20%. Vesicular basaltic vitric fragments are, however, the dominant component at 60% whereas holocrystalline basalt fragments are <10%. Vitric collapsed-pumice fragments are a minor component at ~5%, but are significantly increased in size and abundance from layer A and continue to increase through layer B, reaching several millimeters in size in the coarse layer near its center (Fig. 10). The lower 13 cm of Unit B is massive ash of constant grain size, capped by an even coarser 4-cm-thick ash layer that contains the largest vitric particles. The feldspar crystal size distribution remains constant across Unit B up to this level (Fig. 11). The upper 10 cm of Unit B is vaguely bedded medium ash with another 2-cm-thick layer on top, in which irregular to flattened ellipsoidal greenish vitric particles are abundant.

Unit C

Unit C is 12 cm thick and sharply bounded at top and base. It is overall normally graded, changing from medium ash at the base to fine ash at the top, accompanied by a change from vague bedding near base to fine lamination near the top. This lamination is because of alternating crystal-rich and fossil-rich layers. Collapsed pumices are especially enriched in the fossil-rich layers, where they exceed vesicular basaltic vitric particles in abundance. The major components, however, are 35% fossils (mainly planktonic, minor benthic, and shallow-water bioclasts) and 30% crystals (the typical P1 assemblage plus some phlogopite crystals). Tachylitic and crystalline basalt

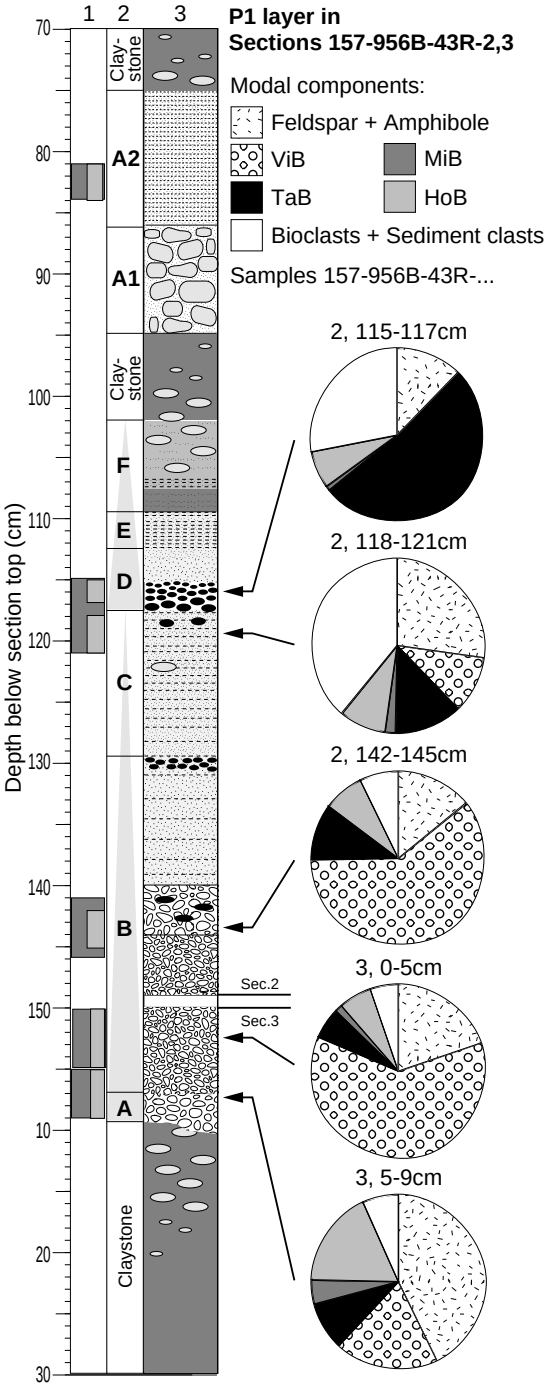

Figure 10. **Left.** Stratigraphic profile of the P1 layer in Hole 956B, subdivided into Subunits A to F. Other features as in Figure 6. **Right.** Modal composition of ash samples. Abbreviations as in Figure 8. Note the abundance of basaltic vitric (ViB) fragments.

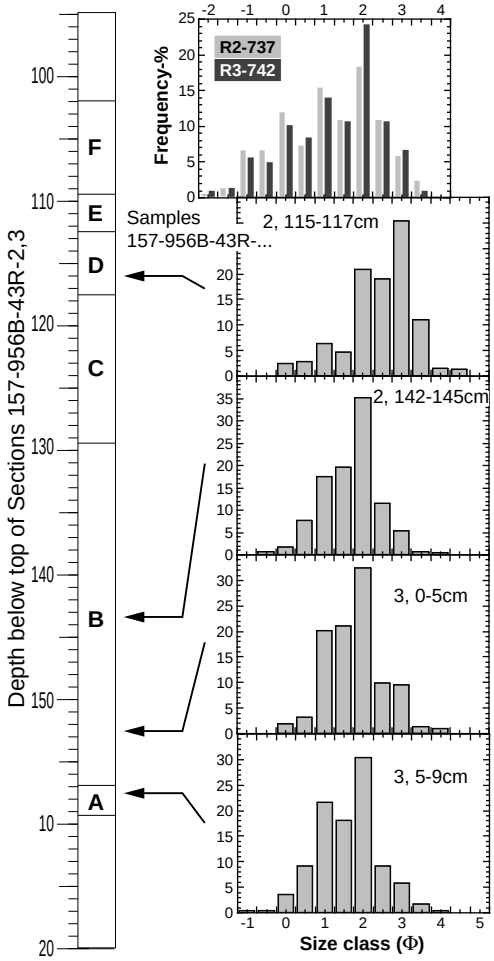

Figure 11. Histograms of feldspar crystal size distributions of P1-layer ash samples from Hole 956B.

fragments reach 20% in total. A 5-mm-long rounded lump of fossil clay is embedded in Unit C, and close to the top some vesicular tachylite lapilli (up to 1 cm long) similar to those in overlying layer D occur.

Unit D

Unit D is a conspicuous 5-cm-thick bed because of the abundance of tachylite lapilli dispersed in a fossil-dominated fine-ash matrix containing crystal, tachylite, and crystalline basalt fragments; neither basaltic nor felsic vitric particles occur in this layer. Some larger feldspar crystals and crystalline basalt fragments contribute to the lapilli fraction, which is, however, vastly dominated by vesicular tachylite lapilli. Textures of these lapilli include anorthoclase or lithic cores in mantled particles and vesicular particles with agglutinated ash rims, particle types that are common in moderately to poorly welded P1 basaltic tuff (Freundt and Schmincke, 1995a). Despite the presence of the large tachylite lapilli, the feldspar crystal size distribution is shifted to finer size (Fig. 11); the median size is only 100 µm compared to 200 µm in Unit B. Layer D is massive and normally graded from tachylite lapilli up to 1 cm in diameter at the base through <1 mm particles in medium ash at the middle to stratified fine ash mixed with fossil clay at the top. Fossils in Unit D are mainly planktonic globigerinoid and some benthic foraminifers.

Unit E

Unit E is 3 cm thick and mainly consists of fossil clay with dispersed ash particles and abundant horizontally aligned, flat, ellipsoidal, probably vitric particles.

Unit F

The 7.5-cm-thick Unit F at the top of the P1 layer also consists of fossil clay mixed with dispersed fine ash.

Ash Layers Above P1

At 30 cm above the P1 layer, the 12-cm-thick finely stratified Subunit A2 consists almost entirely of globigerinoid foraminifers in a clayey matrix. Small fragments (<150 µm) of crystals and tachylitic and crystalline basalt are dispersed in the matrix, but are also enriched in millimeter-thick dark intercalated layers. The crystals comprise anorthoclase and intermediate feldspars (Sample 157-956B-43R-2, 81–84 cm, in Fig. 3C), amphibole of P1 rhyolite, and some other evolved source (Fig. 4E, F), clinopyroxene of basaltic origin (Fig. 5C, F), opaque oxides, and phlogopite.

Layer A3 (60 cm above P1) contains abundant vesicular tachylite and vesicular basaltic vitric fragments, large feldspar, and other crystals (many broken in situ), minor crystalline basalt fragments, and a mixed assemblage of bioclasts. Also present are vitric particles of uncertain origin caused by the absence of phenocrysts. Angular microcrystalline particles with intense flow-banding at microscopic scale, and included anorthoclase, oxide, and zircon crystals are fragments of welded devitrified felsic P1 tuff on land (Pl. 1, Fig. 4). The crystal assemblage mainly composes P1-derived minerals, pyroxenes derived from older basalts, and amphibole derived from ignimbrite R (Sample 157-956B-43R-2, 50–53 cm, in Figs. 3C, 4E, F, and 5C, F). Rare phlogopite crystals do not belong to either P1 or R. Subunit A3 does not contain fine-grained matrix; interparticle voids are partly filled by zeolites.

Layer A5 (105 cm above P1) comprises alternating crystal-rich and fossil-rich layers like A2. Large-scale mixing with overlying fossil clay occurs at the top of the layer. The fine-grained ash (<200 µm) consists of tachylite fragments and crystals of sodic feldspar, amphibole, augite, oxides, zircon, and phlogopite.

SUMMARY AND DISCUSSION OF RESULTS

Magnitude of the P1 Eruption

The volume of pyroclastic material emplaced by the P1 eruption can be roughly estimated by assuming a radial thickness distribution (for details see Freundt and Schmincke, 1992), with an exponential decay fitted to average ignimbrite thicknesses of 30 m at a radial distance of 10 km from the caldera center, that is just outside the caldera, 15 m at 20 km, that is along the island's shore, and 0.3 m at 80 km, that is the most distal ODP drill site (Fig. 1). The latter thickness value is meant to represent P1 material in the core sections, subtracting foreign material and pore space, but considering that P1 material also occurs in reworked ashes postdating the eruption. Accounting also for a hypothetical thickness of 30 m of P1 ignimbrite inside the submarine caldera, the total volume of 83 km^3 DRE now obtained is almost twice that previously deduced from the deposits on land (Freundt and Schmincke, 1992), although this value still does not account for tephra emplaced beyond the drill sites.

Basaltic Accidental Fragments

Highly vesicular basaltic vitric fragments (and a significant fraction of the clinopyroxene crystals) are very abundant in the P1 layer at Site 956 in the southwest and also occur at Site 955 in the southeast, but are very rare at Site 953 in the north (Fig. 1). Such fragments also constitute a major fraction in middle Miocene sandstones at Deep Sea Drilling Project (DSDP) Site 397 (Schmincke and von Rad, 1979). These vesicular fragments were derived from basaltic hyaloclastites (Schmincke and Segschneider, Chap. 12, this volume) emplaced above the volatile fragmentation depth (Fisher and Schmincke, 1984), probably at <800 m (Staudigel and Schmincke, 1984). The holocrystalline dense basalt fragments present at all sites, but predominant in the P1 ash at Holes 955A and 953C, represent an influx of mainly terrigenous detritus (Schmincke and Segschneider, Chap. 12, this volume). The <10% petrographically similar lithic fragments in the P1 ignimbrite on land lack oxidized rims and could not account for the 5%–37% of holocrystalline basalt in the submarine P1 ash.

The Timing of Submarine Emplacement

The coeval basalt fraction is defined as X_{bas} = TaB/(TaB+fsp+am), assuming TaB to represent P1 basalt and fsp+am to represent P1 rhyolite and trachyte. X_{bas} generally increases upward in the P1 layers at Holes 953C and 956B (Fig. 12), although the variation patterns differ. X_{bas} is high at the levels analyzed in the P1 layer at Hole 955A, but the data is yet insufficient to deduce a vertical trend. Also at Holes 953C and 956B, the feldspar crystal content drastically decreases from the bottom of the marine P1 layers upward (Fig. 13). The drop in feldspar content at 953C is coupled with a drop in crystal size (Fig. 14), which generally decreases upward in the P1 layers at both holes. Vertical variations in feldspar content and size are poorly constrained by the present data for Hole 955A, but seem to differ from the variations for Holes 953C and 956B. In the latter two holes, the upward increase of X_{bas} coupled with a decrease of feldspar content and size in the P1 layer roughly corresponds to the vertical compositional variation in the P1 ignimbrite on land, although the detailed patterns of variation are clearly different. If the P1 ignimbrite had been first emplaced in the compositional order observed on land and then been eroded from the top downward or in an

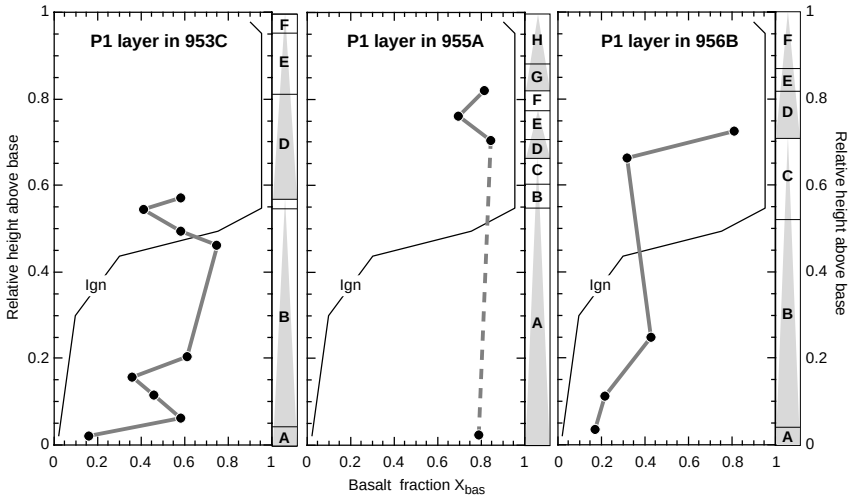

Figure 12. Vertical variation of the fraction of coeval basalt, X_{bas} in the P1 ash layers at the three sites. Height above base is normalized to total thickness. The thin lines show the vertical variation of X_{bas} in the P1 ignimbrite on land. Subunits and cycles are indicated on the right side of each graph for reference.

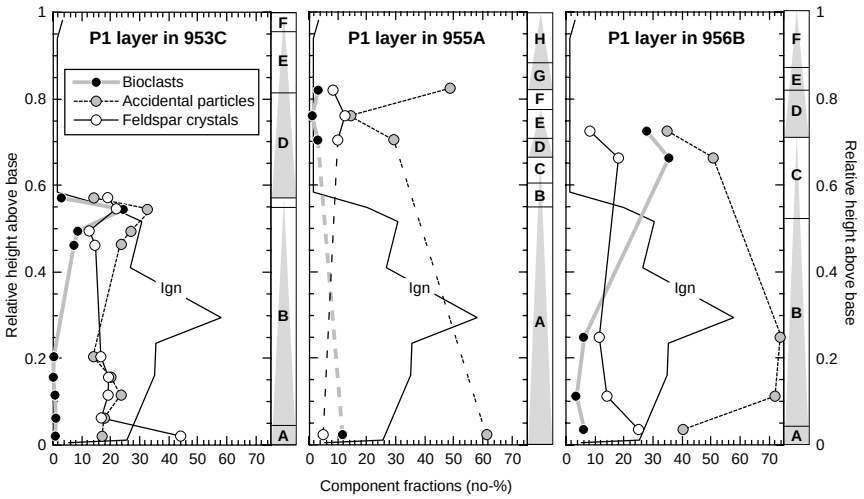

Figure 13. Vertical variation of the modal percentage of bioclasts, total accidental components (i.e., basaltic fragments (HoB and ViB), fossils, clayey sediment clasts), and feldspar crystals, which constitute 74%–99% of the bulk crystal fraction.

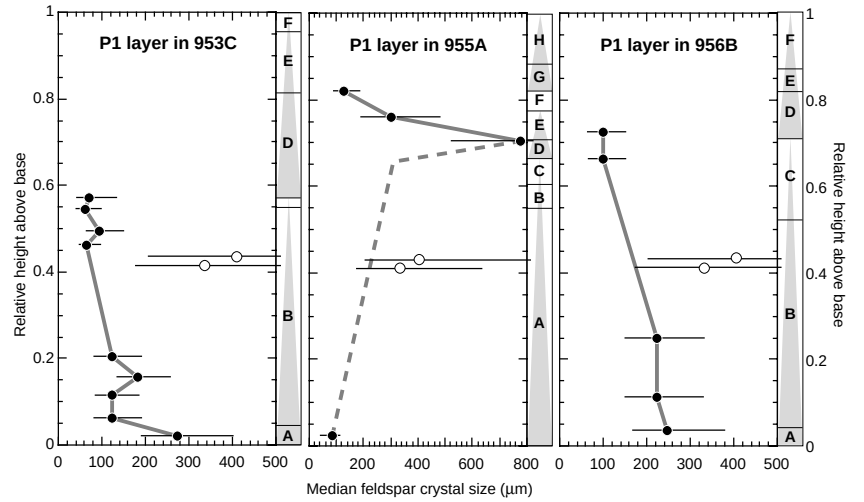

Figure 14. Vertical variation in median feldspar crystal size in the P1 layers. Horizontal bars give the variance as Md±σ. White circles show the median size and variance of feldspar crystals in P1 felsic tuff on land for comparison.

irregular fashion, the reverse order in compositional zonation or chaotic mixing would be expected to occur in the resedimented deposits. The submarine ashes can only reflect the vertical zonation of the ignimbrite if they were formed by progressive accumulation during eruption and emplacement on land. The detailed primary pattern of zonation is bound to get lost, however, when the pyroclastic material passes through a variety of transport processes before it reaches its final submarine location (see below).

There is further evidence in support of our interpretation that submarine deposition was roughly synchronous with subaerial eruption. Anorthoclase and oligoclase crystals contained in the P1 basaltic tuff on land are strongly resorbed with typical fingerprint textures. Freundt and Schmincke (1992) show that this resorption developed during cooling after ignimbrite emplacement. Sodic feldspar contained in basaltic fragments in the submarine P1 layers is generally not resorbed, although we found very thin fingerprint resorption rims on a few crystals. The majority of P1 basalt particles in the submarine ashes are tachylite, whereas the P1 basalt on land is almost entirely crystallized. Both these observations demonstrate that the basalt particles in the submarine P1 layers were rapidly cooled and do not represent eroded P1 basaltic tuff from land. Furthermore, many of the vitric rhyolite and trachyte particles have preserved pumiceous textures (Pl. 2, Figs. 2, 3) no longer found in the highly welded and compacted ignimbrite on land; these vitric particles must have been directly emplaced into water during eruption and therefore escaped welding compaction. Intensely flow-banded microcrystalline fragments that unambigously represent erosional detritus from welded P1 ignimbrite on land do not occur in the P1 layers. They first appear in layer A3 above the P1 layer in Hole 956B (Pl. 1, Fig. 4; Fig. 5). Layer A3 also contains the first crystals derived from subsequent ignimbrite R (Sample 157-956B-43R-2, 50–53 cm, in Fig. 4), which was clearly erupted after complete cooling and local erosion of P1.

Significance of Deformed Vitric Particles

Some of the vitric particles with collapsed-pumice textures have been compacted in a cold state by sediment overload (Pl. 2, Fig. 3). In the majority of these particles, however, long axes of the flattened vesicles are not aligned parallel to bedding. Fragmentation then must have occurred after deformation in a hot viscous state. The flattened vesicles and bended and highly stretched foliations (Pl. 2, Fig. 4) probably formed during viscous compaction. We propose that these fragments represent welded ignimbrite that was disrupted during an early (syndepositional?) stage of compaction, before the densely welded state was reached that characterizes the P1 ignimbrite on land. A possible mechanism of this fragmentation could be steam explosions generated by emplacement of a hot ignimbrite mass into shallow coastal waters. Emplacement may have occurred by rheomorphic viscous creep into the sea, which probably explains the land-to-sea transition of welded Ordovician ignimbrites in Wales and Ireland (Reedman et al., 1987; Fritz and Stillman, 1996). The possibility of emplacement and welding under water of submerged hot ash flows

has also been discussed (Sparks et al., 1980). Alternatively, high accumulation rates of hot pyroclasts sedimenting out of ash flows that move across the surface of the sea may facilitate the formation of welded ignimbrite in shallow water. Whatever the processes of emplacement and disruption were, they operated all around the island because the deformed vitric fragments occur at all three sites.

Significance of Microcrystalline Felsic Particles

In addition to these "general processes," specific conditions must have prevailed at the northern coast of Gran Canaria to create the conspicuous, abundant microcrystalline rhyolitic and trachytic fragments (Pl. 1, Figs. 2, 3) that occur exclusively at Hole 953C. There is no texturally equivalent P1 facies on land that could have served as a source for these particles. The microcrystalline particles do not represent fragments of the welded P1 tuff on land after cooling, because they lack the omnipresent intense microscopic flow banding that resulted from viscous shear before and during devitrification. Pores and vapor-phase mineralization are abundant in the P1 ignimbrite (above the basal vitrophyre), but do not occur in the microcrystalline particles. These are mostly dense, but some contain few oval vesicles. Their angular shapes with straight edges and internal fractures suggest brecciation under thermal stresses. The abundance of these fragments in ash beds more than 60 km off the coast implies that a significant mass of dense, massive, microcrystalline rock was available near the northern shore. This rock mass appears to have been intensely brecciated in a hot state, but it did not experience viscous flow, because flow banding is not observed in the microcrystalline fragments.

We interpret these particles to represent P1 ignimbrite that welded to a dense mass during (not after!) deposition. Rapid cooling probably caused thorough crystallization at high subsolidus temperatures. Crystallization may have inhibited viscous flowage by increasing the viscosity. On the other hand, the absence of such rock facies on land suggests emplacement into water, which could have formed a quenched shell that inhibited viscous deformation. Emplacement into water could also have provided the thermal stresses required for intense brecciation. But how did this emplacement process work, how does it differ from that producing the vitric fragments discussed above, and why did it only operate in the north of the island?

In the absence of any evidence from near the coast, our explanations remain speculative. A possible answer may be found in the context of the difference in topography between the north and south of the island. Although a flat and wide coastal lowland characterized the paleo-topography in the south, deep narrow radial canyons appear to have prevailed in the north. The present-day shelf is quite extensive in the south but narrow in the north (Fig. 1), and a similar shelf distribution may have been present at 14 Ma. Such a topographic situation would lead to shallow-angled, widely distributed entrance of the ash flows into extensive shallow water in the south, but to locally very high accumulation rates of hot ash from channelized ash flows entering the sea through radial canyons in the north. We propose that hot pyroclastic material from the P1 ash flows accumulated so rapidly on the shelf and upper flank in the north that it replaced the water and was able to weld to a dense mass. Viscous deformation of the mass, which occurred synchronous with deposition on land, may have been delayed by marginal chilling. Instability caused by the rapid and massive emplacement triggered landsliding and brecciation (facilitated by thermal stresses) of the crystallizing mass of ignimbrite, especially that resting close to the edge of the narrow shelf. Lower local accumulation rates because of wider spreading of the ash flows, may have inhibited such processes in the south, where only vitric particles formed as discussed above.

Depositional Cycles

The P1 layers of Holes 953C and 956B, northeast and southwest of Gran Canaria, can be interpreted to each comprise two cycles of deposition. The first cycles (Units A–C in both sections; Figs. 6, 10) begin with a coarse-grained crystal-rich basal layer followed by massive to weakly bedded ash, which is almost devoid of fine-grained matrix. Grain size decreases upward (Fig. 14), where fine matrix appears and increases in abundance. The fossil content also increases upward (Fig. 13) and changes from a shallow-water, benthic, and planktonic mixed assemblage near base to a dominantly planktonic population near top. Bedding improves upward to finally form alternating crystal-rich and fossil-rich laminations at the top of the cycle. The crystal content varies little above basal Unit A. The same holds for noncoeval basalt fragments in Hole 953C (mainly HoB), whereas those in Hole 956B (mainly ViB) decrease upward (Fig. 13). The second cycles (Units D–F in both sections) also begin with coarse-grained layers and become finer upward. The base of the second cycle is formed by matrix-free medium ash in Hole 953C, but by large normally graded tachylite lapilli in a fine-grained matrix in 956B. The overall vertical evolution is, however, characterized by normal grading, improved bedding from massive through low-angle cross-bedding to fine lamination, and an increasing and finally dominant fossil-clay component. Shallow-water and benthic fossils typically occur near base of the cycle, but the entire population is dominated by planktonic globigerinoid foraminifers.

The P1 layer at Site 955, southeast of Gran Canaria, comprises three depositional cycles including Units A–C, D and E, and G and H, respectively (Fig. 8). Fines depletion is observed in the lower parts of the first and third cycles. Fine matrix at the very base of the first cycle (Unit A) is fossil clay incorporated by erosion of the substratum. The base of the first cycle lacks the very coarse-grained and highly crystal-rich basal layer that is so prominent in Holes 953C and 956B (Figs. 13, 14); the entire section of Hole 955A is rather crystal-poor but dominated by tachylitic basalt (Figs. 8, 12, 13). The top of the first cycle (Unit C) differs from that at the other sites by being composed of massive fossil clay mixed with small crystal fragments. We do not believe, however, that this layer indicates a significant time break between the first and second cycles, because the admixed crystals suggest that Unit C represents resedimented rather than primary pelagic clay. The base of the second cycle (Unit D) is conspicuous by its high content of weakly normally graded tachylite lapilli set in a fine-grained matrix, and correlates with the base of the second cycle (Unit D) at Site 956, although it does not contain as abundant fossils (Figs. 8, 10). The entire P1 layer at Site 955 is, however, poor in fossils compared to the sections from the other sites (Fig. 13). The third cycle shows topward increased mixing with fossil clay similar to the top of the P1 layer at Site 956. The second and third cycles are separated by the very fine-grained, crystal- and fossil-poor, massive layer F (Fig. 8) that contains abundant small basaltic shards; this layer clearly represents a depositional event separate from those forming the coarser grained depositional cycles.

Vertical variations similar to those of the depositional cycles of the P1 layers also characterize most of the ash beds below and above the P1 layers. Ash pockets intruded into underlying fossil clay, and wavy or concave-up basal contacts appear to be syndepositionally formed flute marks and load casts as well as convolute bedding that resulted from rapid emplacement of the higher-density, sand-sized layers onto unconsolidated clay. Similar mixing structures with overlying fossil clay at the top of some ash layers, on the other hand, probably formed some time after emplacement as a result of increased pore pressure in the sand-sized beds during compaction.

Ash-Layer Emplacement

Normal overall grading, the variations in bedding structures, the top and bottom marks and casts, and the abundance of shallow-water bioclasts are typical for turbidites (Allen, 1984). Furthermore, the absence of inverse grading (i.e., grain dispersive pressures), the absence of significant particle rounding, the good sorting, and the preserva-

tion of fragile vesicular particles argue against a high-friction grain-flow transport as in debris flows (cf. Schmincke and von Rad, 1979).

The two to three cycles were emplaced by separate turbidity currents in rapid succession, as indicated by the lack of intervening pelagic clay. The first currents were stronger and of higher mass flux, depositing thicker, coarser, and better sorted massive units (Bouma division A) before waning flow strength allowed for the formation of bedding and deposition of fine grains (Komar, 1985). The absence of fine matrix from the lower portions of the first cycles is, however, unusual for turbiditic sediments. Normally, both coarse and fine particles deposit simultaneously from a turbidity current, either because a hyperconcentrated basal depositional zone evolves or because fine grains are trapped between settling coarser particles (Kneller and Branney, 1995; Komar, 1985). Some process must have operated to efficiently separate the coarse- and fine-grain populations. The three drill sites were placed only a few kilometers away from the base of the steep submarine flanks of Gran Canaria on the flat floor of the adjacent basins (Figs. 1, 15). The Froude number of turbidity currents, $Fr = [\sin \alpha/(1+a)C_f]^{1/2}$ with α = slope, a = 0.8 top to bottom stress ratio, and drag coefficient $C_f = 0.005$ (Komar, 1971), would be 3.7 to 4.2 (supercritical) on the average flank slopes of 7°–9° but would drop to subcritical values Fr<1 on basin slopes <0.5°. This critical slope was probably reached in the vicinity of the three drill sites (Fig. 15). The ash layers were thus emplaced close to where the turbidity currents passed through hydraulic jumps in their transition from supercritical to subcritical flow. The intensity of turbulent mixing with ambient water involved in such jumps increases with pre-jump Froude number (Komar, 1971). The turbulence intensity implied by the high Fr-values on the submarine flanks of the island would allow for efficient separation of the coarse and fine particle loads.

The increasing fossil and fossil-clay component toward the top of each cycle probably represents material that was stirred up from the ocean floor by the turbidity currents and resedimented from a turbid cloud left behind by the current. Voids in the planktonic fossil shells are filled with clay suggesting that they had previously rested in clayey sediment. Rare empty shells, on the other hand, may represent organisms that were still floating alive in the water admixed to the turbidity current. These organisms were then trapped between settling clastic particles during deposition. Upslope of Hole 955A, the turbidity currents appear to have disturbed fine-grained hyaloclastite deposits, which slumped to generate a suspension forming Unit F in the respective P1 layer. This suspension must have had a very restricted source region and did not erode during transport, because the deposit has a very homogeneous composition.

As argued above, turbidite emplacement seems to have occurred more or less concurrently with eruption of the P1 ignimbrite. The abundance of shallow-water fossil fragments and of holocrystalline basalt fragments, representing epiclastic terrigeneous material that had most likely accumulated on the flat shelf around the island, shows that the prime material source of the turbidity currents must have been very close to shore. Considering that holocrystalline basalt fragments account for 5%–37% of the P1 ash, of which only a few percent can be attributed to the lithic fraction carried by the P1 ash flows, the implication is that several cubic kilometers of basaltic detritus must have been moved off the shelf. A similarly large bulk volume must be attributed to the 10%–60% basaltic vitric fragments in the P1 layers at Sites 956 and 955. It is unlikely that such large volumes have been remobilized by erosion through turbidity currents at an early stage of their evolution high on the island's flanks. More likely, the massive input of pyroclastic material into shallow water by the ash flows could have caused mass sliding and debris flows off the shelf, which subsequently transformed into turbidity currents (Hampton, 1972; Fisher 1984; Garcia and Meyerhoff Hull, 1994).

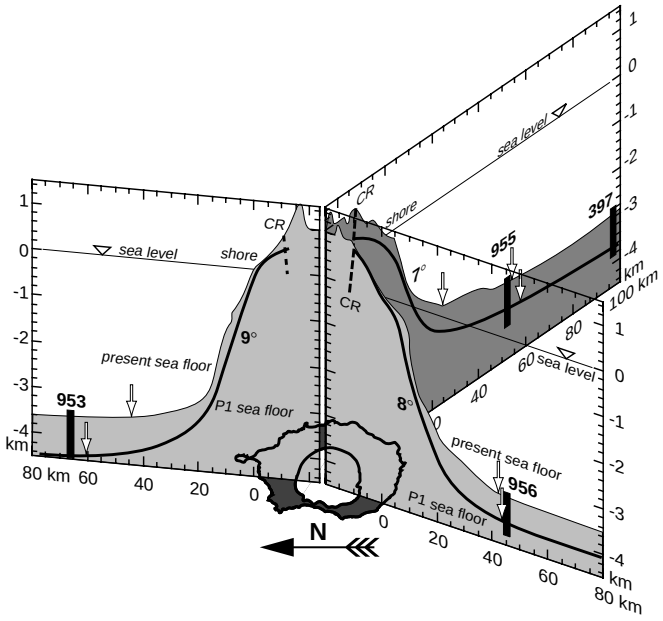

Figure 15. Vertically exaggerated radial cross sections based on the bathymetry in Figure 1. Vertical black bars = Sites 953, 955, 956, and DSDP Site 397. Thick lines = ocean floor at the time of P1 emplacement. Dashed lines = caldera rim (CR) on the island. Submarine flanks of Gran Canaria have average slopes of 7°–9°. White arrows = points where the critical slope of 0.5° is reached on the present floor and on the paleosurface, where exact positions cannot, however, be determined for the lack of paleobathymetric data.

Did Coastal Explosions Occur?

One of the most hazardous ways in which hot pyroclastic flows can interact with the seawater are steam explosions (Cas and Wright, 1991). The submarine P1 layers provide some indications that such explosions occurred. The ratio of feldspar crystals to coeval felsic vitric material in the P1 layers is 3–5, whereas it is <1.3 in the felsic P1 tuff on land. This may partly be because of the difficult recognition of vitric material altered to clay, but even if we calculate the ratio of feldspar crystals to all clayey matrix that is not obviously fossil clay, we obtain values significantly larger than 1.3. Vitric material therefore must have been effectively separated from crystals. Large vitric particles appear to have been highly pumiceous and thus would have been easily separated in the water to be deposited at some place not sampled by drilling (e.g., Carey et al., 1996; Whitham, 1989; Mandeville et al., 1996). The median size of feldspar crystals in the P1 layers is variable but up to four times smaller than in the ignimbrite on land (Fig. 14). Their better sorting (around σ = 0.8) compared to the ignimbrite crystals (σ = 1.4) is mainly caused by a loss of coarse crystals (Figs. 7, 9, 11). The straight-forward explanation for this observation is hydraulic sorting during transport, that is, loss of the coarser crystals from the turbidity currents at more proximal locations. This must clearly have been the case, but it does not explain why fine-grained ash samples show feldspar modes at +3 and +3.5 ϕ (125 and 88 µm), whereas this fine size class is almost absent in the ignimbrite, and why the occurrence of large tachylite lapilli is not associated with correspondingly large feldspar crystals, with the exception of Unit D in Hole 955A. We suggest that the abundance of fine feldspar fragments in the submarine ashes is partly because of fragmentation of feldspar crystals during the explosive interaction of the hot ash flows with the cold seawater. Such interaction could have finely fragmented much of the vitric material, facilitating its separation from crystals and transport in dilute suspension to become distributed over a vast area and thus difficult to identify in the sedimentary record. Explosive interaction of ash flows with water could have been a trigger for instability and the slumping of sediment masses off the shelf.

Did Pyroclastic Flows Move Over Water?

Based on experimental and theoretical considerations, Freundt (1995) argues that hot ash flows, which form high-grade ignimbrite, must move as considerably expanded flow. Geologic evidence in favor of an expanded mode of transport of the ash flows that generated the basaltic upper part of ignimbrite P1 on land is discussed by Freundt and Schmincke (1995a). A vertical gradient of downward increasing particle concentration of such ash flows may facilitate their separation into two parts upon reaching the sea, one part intruding into the water, the other part continuing to move over the water. Carey et al. (1996) and Mandeville et al. (1996) provide compelling evidence that such a separation occurred during the 1883 Krakatau eruption. Some indication that P1 ash flows moved over water comes from the large tachylite lapilli, which are primary pyroclastic particles of the basaltic P1 ash flows. These tachylite lapilli are strongly enriched in some layers, but also occur dispersed in the submarine P1 ash sections. They are not in hydraulic equilibrium with the fine-grained foraminifer-rich matrix that encloses them (e.g., Unit D in Hole 956B; Fig. 10). They rather appear to be outsized additions to the turbidity currents that emplaced the matrix material. We propose that the tachylite lapilli represent pyroclastic material that was lost from ash flows moving over the sea, settled through the water, and mixed with the finer load of synchronous turbidity currents. The P1 layers may actually also contain a significant amount of finer P1 pyroclastic material sedimented in this fashion, but there is no way to distinguish it from that initially contained in the turbidity currents.

CONCLUSIONS

The 44- to 86-cm-thick volcaniclastic P1 layers at Sites 953, 955, and 956 around Gran Canaria correspond stratigraphically to the mixed rhyolite-trachyte-basalt welded ignimbrite cooling unit P1 on land, as shown by mineral compositions. The first ascertained appearance of material from subsequent ignimbrite R is in ash layer A3 in Hole 956B, 60 cm above the P1 layer (Fig. 2). A minor contribution from evolved precursor rocks to the P1 ash, and possibly to layer B2 below it in Hole 956B, is indicated by the composition of some crystals.

The P1 layers were emplaced by two to three turbidity currents in water depths of 3420 to 4420 m. Several lines of evidence show that submarine emplacement of the P1 layers occurred concurrently with the eruption on land. Primary pyroclastic material delivered to the sea by the hot ash flows was mixed with a huge amount (up to 70%) of foreign material that comprises terrigenous basaltic detritus, vesicular hyaloclastite-derived fragments, as well as shallow-water, benthic and planktonic bioclasts. This material was probably mobilized by mass slumping on the shelf and upper submarine flank of the island, triggered by the massive influx of pyroclastic material through the ash flows (Fig. 16). Fragmentation of crystals and effective separation of coeval felsic glass suggest that explosive interaction of the hot ash flows with seawater (e.g., Cas and Wright, 1991) may have facilitated sediment instability. On the 7°–9° steep flanks of the island, the slumping debris flows transformed into supercritical turbidity currents that passed through hydraulic jumps upon impingement on the flat floor of the adjacent basins (Fig. 16). These jumps probably occurred close to the drill sites and caused the extremely fines-depleted character of the massive (Bouma A) divisions of the deposits. The expanded portions of the hot P1 ash flows probably traveled across the water, continuously losing pyroclastic material that added to the material simultaneously emplaced by turbidity currents (Fig. 16). The large tachylite lapilli enriched in layers with finer matrix may have been emplaced in this way.

Felsic vitric fragments in the P1 layers have all altered to clay, but have preserved variably vesicular textures that indicate some compaction and stretching in a viscous state. Flow banding down to microscopic scales, which is ubiquitous in the ignimbrite on land, is not found in the vitric particles. Viscous flowage during welding therefore was not important during ignimbrite emplacement in coastal seawater. Fragmentation and resedimentation of the ignimbrite mass rather appears to have interrupted the welding process well before compaction eliminated the vesicles, as it did on land. Explosive fragmentation was probably generated by contact of either the ash flows

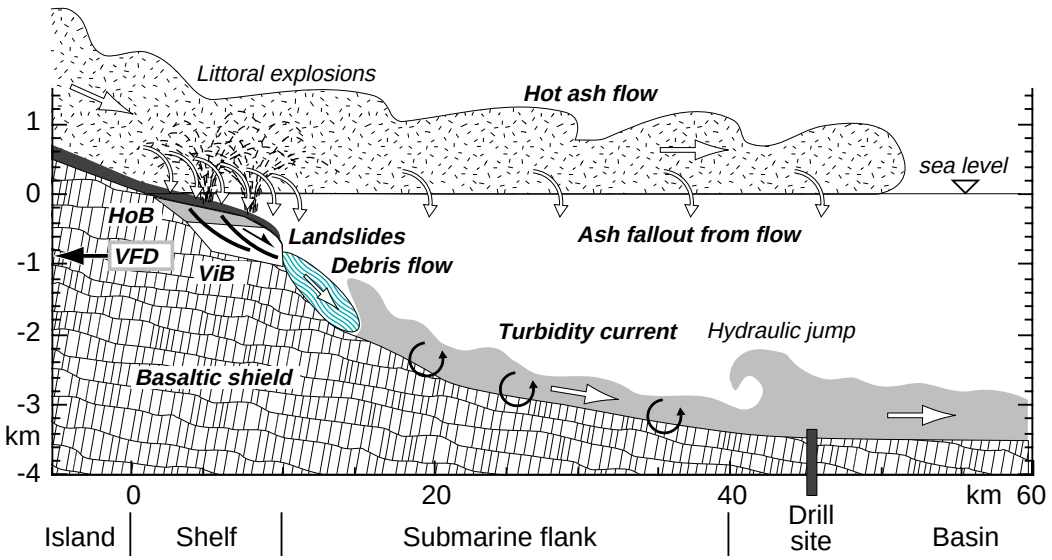

Figure 16. Schematic illustration of the sequence of processes proposed to have led to the formation of P1 layers at the ODP drill sites. Sediments on and below the shelf include vesicular hyaloclastites (ViB, white) formed above the volatile fragmentation depth (VFD) and were capped by a wedge of epiclastic basalt fragments (HoB, gray). Shelf and subshelf deposits became unstable during massive deposition from the P1 ash flows and possibly by littoral explosions, continuously slumping off the shelf and transforming through debris flows into turbidity currents on the submarine flanks, which passed through hydraulic jumps on the flat basin floor and stirred up ocean-bottom sediments subsequently emplaced in the fine-grained top zone of each depositional cycle.

themselves or the just emplaced ignimbrite with seawater. Distribution of the ash flows across the wide coastal lowland and the extensive shelf in the south of Gran Canaria probably facilitated intense interaction with seawater.

The exclusive occurrence of abundant angular, microcrystalline, non- to poorly vesicular rhyolitic and trachytic particles in the P1 layer at Site 953 implies special conditions during the entrance of ash flows into the sea north of Gran Canaria. These particles represent a fairly dense mass of ignimbrite that had become thoroughly devitrified and fragmented by thermal stresses before rheomorphic viscous deformation could commence. We speculate that extremely high local accumulation rates in shallow water from ash flows channeled through radial canyons to the north of Gran Canaria allowed the formation of a welded ignimbrite mass on the narrow shelf, probably extending onto the upper submarine flank. Marginal chilling delayed viscous flowage until this mass slumped off the shelf and brecciated before the onset of rheomorphism.

Several ash layers containing P1 material, which were also emplaced by turbidites, occur above the P1 layers at the three sites, but are separated by fossil claystone, indicating time intervals of order 10^2 years between turbidite generation and emplacement. The first appearance of epiclastic detritus derived from the P1 ignimbrite on land coincides with the first appearance of crystals derived from subsequent ignimbrite R, which was erupted after P1 had completely cooled and been locally eroded.

ACKNOWLEDGMENTS

We thank Walter Hale for assisting at BCR, Wolf-Christian Dullo for helping to identify the bioclasts, and Marianne Stavesand for assisting in sample preparation and analysis. Helpful comments on an earlier version by Nancy Riggs, an anonymous reviewer, and editor Bob Wathen, are much appreciated. This work was funded by grants from the Deutsche Forschungsgemeinschaft to AF (Fr947/5-1) and HUS (Schm250/47-1).

REFERENCES

Allen, J.R.L., 1984. *Sedimentary Structures: Their Character and Physical Basis.* Developments in Sedimentology, 30: Amsterdam (Elsevier).

Carey, S., Sigurdsson, H., Mandeville, C., and Bronto, S., 1996. Pyroclastic flows and surges over water: an example from the 1883 Krakatau eruption. *Bull. Volcanol.,* 57:493–511.

Cas, R.A.F., and Wright, J.V., 1991. Subaqueous pyroclastic flows and ignimbrites: An assessment. *Bull. Volcanol.,* 53:357–380.

Fisher, R.V., 1984. Submarine volcaniclastic rocks. *In* Kokelaar, B.P., and Howells, M.F. (Eds.), *Marginal Basin Geology: Volcanic and Associated Sedimentary Processes in Modern and Ancient Basins.* Geol. Soc. Spec. Publ. London, 16:5–28.

Fisher, R.V., and Schmincke, H.-U., 1984. *Pyroclastic Rocks:* New York (Springer-Verlag).

Freundt, A., 1995. On the transport mechanisms of hot ash flows. *IUGG XXI General Assembly, Boulder, USA, Abstract Vol.,* B410. (Abstract)

Freundt, A., and Schmincke, H.-U., 1992. Mixing of rhyolite, trachyte and basalt magma erupted from a vertically and laterally zoned reservoir, composite flow P1, Gran Canaria. *Contrib. Mineral. Petrol.,* 112:1–19.

————, 1995a. Eruption and emplacement of a basaltic welded ignimbrite during caldera formation on Gran Canaria. *Bull. Volcanol.,* 56:640–659.

————, 1995b. Petrogenesis of rhyolite-trachyte-basalt composite ignimbrite P1, Gran Canaria, Canary Islands. *J. Geophys. Res.,* 100:455–474.

Fritz, W.J., and Stillman, C.J., 1996. A subaqueous welded tuff from the Ordovician of County Waterford, Ireland. *J. Volcanol. Geotherm. Res.,* 70:91–106.

Funck, T., 1995. Aufbau des nördlichen vulkanischen Schuttfächers Gran Canarias ermittelt aus reflexionsseismischen und anderen geophysikalischen Daten. [Ph.D. dissertation]. Geomar, Kiel.

Garcia, M.O., and Meyerhoff Hull, D., 1994. Turbidites from giant Hawaiian landslides: results from Ocean Drilling Program Site 842. *Geology,* 22:159–162.

Hampton, M.A., 1972. The role of subaqueous debris flow in generating turbidity currents. *J. Sediment. Petrol.,* 42:775–793.

Hoernle, K., and Schmincke, H.-U., 1993. The petrology of the tholeiites through melilite nephelinites on Gran Canaria, Canary Islands: crystal fractionation, accumulation, and depth of melting. *J. Petrol.,* 34:573–578.

Kneller, B.C., and Branney, M.J., 1995. Sustained high-density turbidity currents and the deposition of thick massive sands. *Sedimentology,* 42:607–616.

Komar, P.D., 1971. Hydraulic jumps in turbidity currents. *Geol. Soc. Am. Bull.,* 82:1477–1488.

————, 1985. The hydraulic interpretation of turbidites from their grain sizes and sedimentary structures. *Sedimentology,* 32:395–407.

Mandeville, C.W., Carey, S., and Sigurdsson, H., 1996. Sedimentology of the Krakatau 1883 submarine pyroclastic deposits. *Bull. Volcanol.,* 57:512–529.

Reedman, A.J., Howells, M.F., Orton, G., and Campbell, S.D.G., 1987. The Pitts Head Tuff Formation: a subaerial to submarine welded ash-flow tuff of Ordovician age, North Wales. *Geol. Mag.,* 124:427–439.

Schmincke, H.-U., 1976. The geology of the Canary Islands. *In* Kunkel, G. (Ed.), *Biogeography and Ecology in the Canary Islands:* The Hague (W. Junk), 67–184.

Schmincke, H.-U., 1982. Volcanic and chemical evolution of the Canary Islands. *In* von Rad, U., Hinz, K., Sarnthein, M., and Seibold, E. (Eds.), *Geology of the Northwest African Continental Margin:* Berlin (Springer), 273–306.

————, 1993. *Geological Field Guide: Gran Canaria:* Witten (Pluto Press).

Schmincke, H.-U., and von Rad, U., 1979. Neogene evolution of Canary Island volcanism inferred from ash layers and volcaniclastic sandstones of DSDP Site 397 (Leg 47A). *In* von Rad, U., Ryan, W.B.F., et al., *Init. Repts. DSDP,* 47 (Pt. 1): Washington (U.S. Govt. Printing Office), 703–725.

Schmincke, H.-U., Weaver, P.P.E., Firth, J.V., et al., 1995. *Proc. ODP, Init. Repts.,* 157: College Station, TX (Ocean Drilling Program).

Sparks, R.S.J., Sigurdsson, H., and Carey, S.N., 1980. The entrance of pyroclastic flows into the sea. II: Theoretical considerations on subaqueous emplacement and welding. *J. Volcanol. Geotherm. Res.,* 7:97–105.

Staudigel, H., and Schmincke, H.-U., 1984. The Pliocene seamount series of La Palma/Canary Islands. *J. Geophys. Res.,* 89:11195–11215.

Whitham, A.G., 1989. The behaviour of subaerially produced pyroclastic flows in a subaqueous environment: Evidence from the Roseau eruption, Dominica, West Indies. *Mar. Geol.,* 86:27–40.

Date of initial receipt: 3 July 1996
Date of acceptance: 6 January 1997
Ms 157SR-112

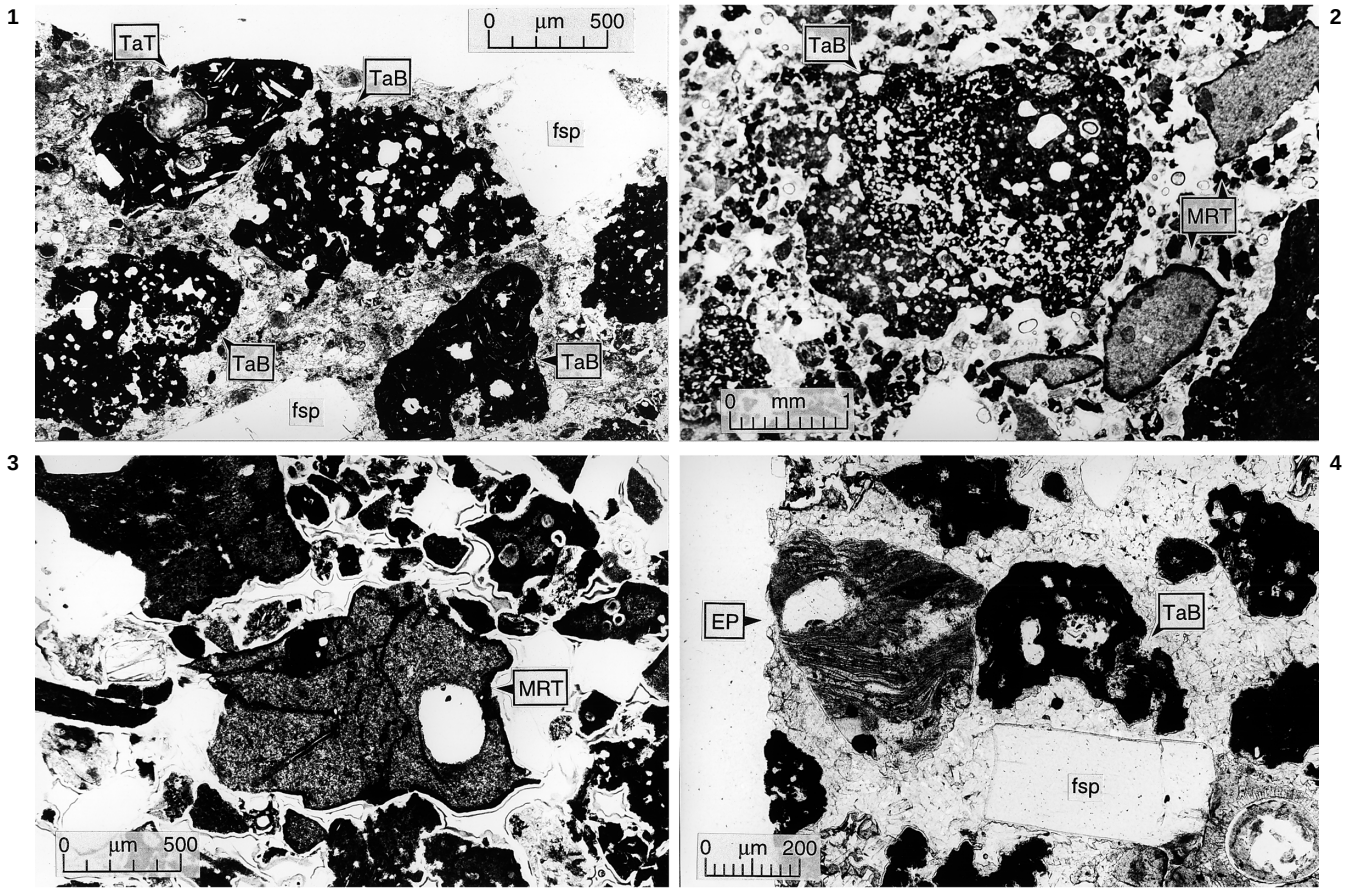

Plate 1. Photomicrographs. **1.** Ellipsoidal mafic trachytic to trachyandesitic tachylite particle (TaT) containing oligoclase and augite microphenocrysts (upper left) and vesicular basaltic tachylite particles (TaB; Sample 157-956B-43R-2, 115–117 cm). **2.** Composite vesicular tachylite particle (TaB) typical of the P1 basaltic tuff, and angular microcrystalline particles (MRT) with thin dark rim (Sample 157-953C-70R-2, 124–127 cm). **3.** Internally fractured microcrystalline rhyolitic particle (MRT) containing anorthoclase and Fe-Ti oxide intergrown with zircon and apatite (Sample 157-953C-70R-3, 15.5–19 cm). **4.** Microflow-banded epiclastic fragment (EP) of welded felsic P1 tuff, basaltic tachylite particles (TaB), euhedral feldspar crystal (fsp), and globigerinoid foraminifer (lower right corner) in zeolite matrix of layer A3 above the P1 layer (Sample 157-956B-43R-2, 50–53 cm; Fig. 5).

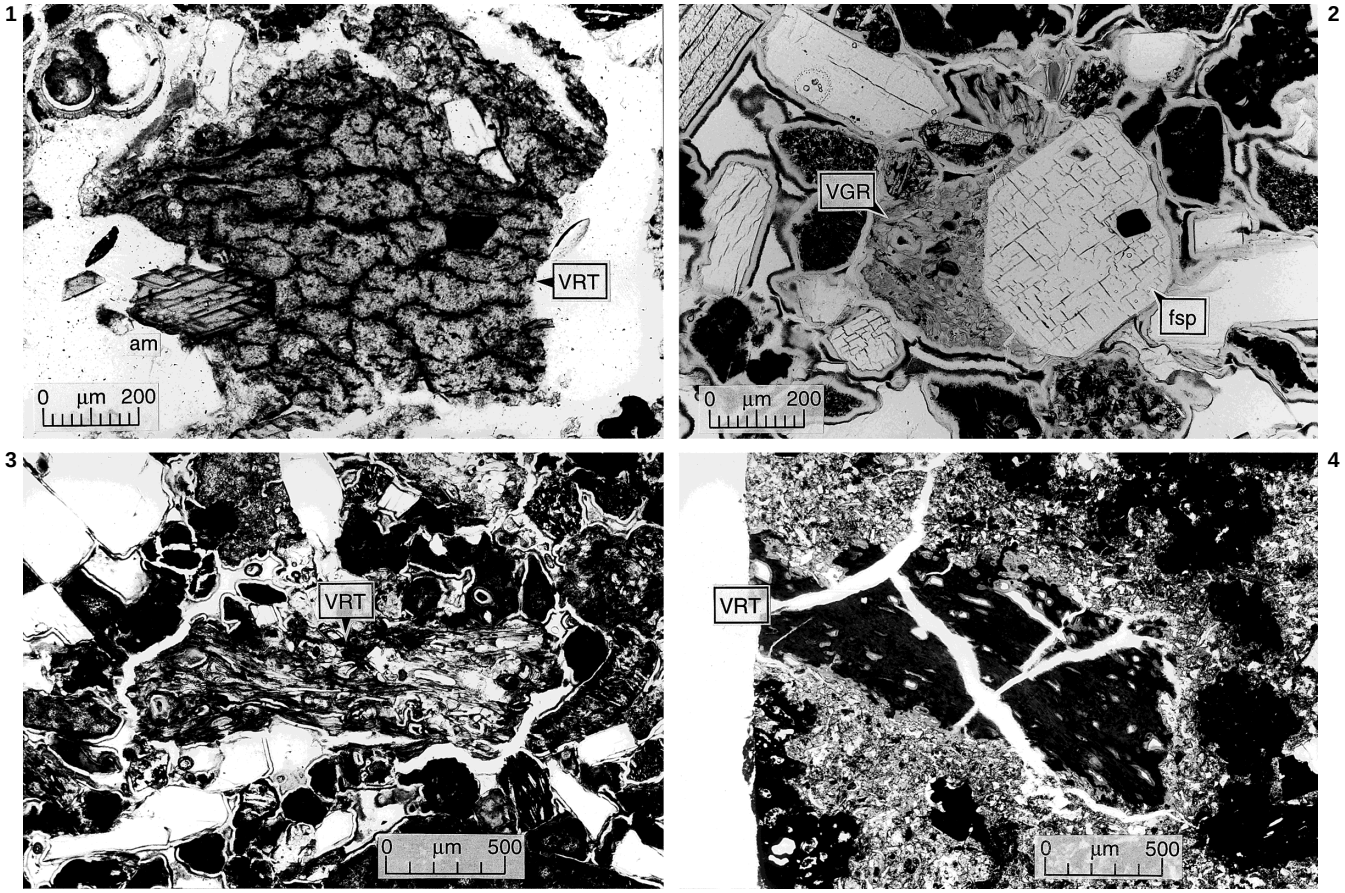

Plate 2. Photomicrographs. **1.** Vitric rhyolite particle (VRT) altered to clay and containing edenite (am) phenocryst (Sample 157-956B-43R-2, 118–121 cm). The network of black lines possibly reflects collapsed vesicles. **2.** Vesicular glass rim (VGR; gone to clay) on anorthoclase (fsp) crystal (Sample 157-953C-70R-3, 12–15.5 cm). **3.** Pumiceous vitric particle (VRT) collapsed in situ by compaction (Sample 157-953C-70R-3, 4–7 cm). **4.** Vitric fragment (VRT) with partially collapsed vesicles and intense lineations reflecting stretching and bending, probably a fragment of welded tuff disrupted at an early stage of welding compaction (Sample 157-955A-60X-3, 145–146.5 cm).

Prior Chapter Contents Next Chapter